

# The Case for positron polarisation at a LC Status Report\*

POWER WORKING GROUP<sup>1</sup>

<sup>1</sup> *institues*

---

\*For further informations, see <http://www.ippp.dur.ac.uk/~gudrid/power/write-up> . For questions and comments, please contact [g.a.moortgat-pick@durham.ac.uk](mailto:g.a.moortgat-pick@durham.ac.uk) .

# Contents

<b>1</b>	<b>Introduction</b>	<b>6</b>
1.1	General remarks about the structure of couplings (not complete) . . . . .	6
1.2	Longitudinally polarised Electrons (under work) . . . . .	8
1.3	Improvement of effective Polarisation (not yet final) . . . . .	8
<b>2</b>	<b>Physics with Polarisation of <math>e^-</math> and <math>e^+</math> beam</b>	<b>12</b>
2.1	Determination of quantum numbers of new physics particles . . . . .	12
2.2	Suppression of Background Channels	
	3 examples (under work) . . . . .	14
2.2.1	$e^+e^- \rightarrow W^+W^-$ . . . . .	14
2.2.2	$e^+e^- \rightarrow \nu\nu\gamma$ : example ED, $e^+e^- \rightarrow \gamma G$ . . . . .	14
2.2.3	Susy example: Smuon production, Uriel . . . . .	14
2.3	Model-independent contact-interaction analysis at LC: role of electron and positron polarizations . . . . .	14
2.4	Determination of sfermion parameters . . . . .	23
2.5	Sfermion Mass measurements in the continuum (will be written by Uriel) . . . . .	26
2.6	CP asymmetries in Neutralino Production and 2-body decay . . . . .	26
2.7	CP asymmetries in Neutralino Production and 3-body Decay . . . . .	30
2.8	Production of Singlino-dominated Neutralinos with Polarized Beams . . . . .	34
2.9	Polarization effects in R-parity violating SUSY . . . . .	36
2.10	Production of heavy Higgs bosons in weak boson fusion . . . . .	38
2.11	Triple gauge boson couplings . . . . .	39
2.12	Probing New Physics with Transverse Polarization via CP violation (plots+some more text are coming) . . . . .	42
2.13	Transverse Polarization and Extra Dimensions at Linear Colliders . . . . .	43
2.14	Separation of light flavors with transverse polarisation . . . . .	54
2.15	Polarisation Measurement: GigaZ – Precision tests of the electroweak theory	56
	2.15.1 Introduction . . . . .	56
	2.15.2 Higgsmass versus electroweak mixing angle . . . . .	58
2.16	Summary of the Physics Cases . . . . .	60
<b>3</b>	<b>Implementation of Spin Effects in Monte Carlo Generators</b>	<b>61</b>
3.1	General-purpose Event Generators . . . . .	62
3.2	Parton-Level Event Generators . . . . .	63
3.3	SUSY . . . . .	64

<b>4</b>	<b>Machine Issues</b>	<b>65</b>
4.1	Electron Polarisation . . . . .	65
4.2	Positron Polarisation . . . . .	65
4.2.1	Helical undulator design at Daresbury . . . . .	66
4.3	Transverse Polarisation . . . . .	68
<b>5</b>	<b>Polarisation Measurement</b>	<b>69</b>
5.0.1	NLC polarimeter, draft . . . . .	70
<b>6</b>	<b>Summary and Outlook</b>	<b>76</b>

# List of Figures

1	Effective polarization as a function of the beam polarization. . . . .	8
2	Polarisation uncertainty in $\sigma$ and $A_{FB}$ . . . . .	9
3	$P(e^+)$ effects in contact interaction and $Z'$ studies . . . . .	10
1	Selectrons: quantum number separation . . . . .	13
2	CI versus integrated luminosity . . . . .	16
3	CI versus integrated luminosity for muons . . . . .	16
4	97% CL range for CI couplings . . . . .	18
5	95% CL for CI scale in Bhabha scattering . . . . .	19
6	95% CL for CI scale in Moeller scattering . . . . .	20
7	$5\sigma$ reach on the mass scale $M_H$ versus luminosity . . . . .	22
8	Production of $\tilde{t}_1\tilde{t}_1$ with polarised beams . . . . .	24
9	Determination of stop parameters via cross sections and $A_{LR}$ . . . . .	24
10	T-odd asymmetry for different neutralino production . . . . .	27
11	CP asymmetries for Neutralino production and decay into taus . . . . .	28
12	CP asymmetries for Neutralino production and decay into taus . . . . .	29
13	CP asymmetries in Neutralino Production and Decay . . . . .	31
14	Singlino-dominated Neutralino Production . . . . .	35
15	R-parity violating Susy: sneutrino production . . . . .	36
16	Differential azimuthal asymmetries in the ADD model . . . . .	46
17	5 sigma identification reach for the mass scale . . . . .	48
18	5 sigma identification reach for the mass scale . . . . .	48
19	Azimuthal distribution . . . . .	50
20	5 sigma reach for nonzero region of azimuthal asymmetry . . . . .	51
21	Transverse polarisation asymmetry in WW production . . . . .	52
22	Transverse polarisation asymmetry for $\gamma\gamma, ZZ$ production . . . . .	52
23	Flour separation with transversely polarised beams . . . . .	55
24	GigaZ: Left-right asymmetry . . . . .	57
25	GigaZ: $\sin^2 \theta_{eff}^l$ versus $M_W$ . . . . .	57
26	GigaZ: Higgs mass versus leptonic eff. mixing angle . . . . .	58

# List of Tables

1.1	Possible different spin configurations in $e^+e^-$ . . . . .	8
2.1	Chosen Parameters for Neutralino Production in 2.2.5.4 . . . . .	33
2.2	Sneutrino production rates versus Bhabha scattering . . . . .	37
2.3	CP conserving triple gauge couplings . . . . .	39
2.4	Imaginary parts of triple gauge couplingsa . . . . .	40
2.5	Identification reach for mass scale in ADD model . . . . .	49
2.6	Search reach for new mass scale . . . . .	49

# Chapter 1

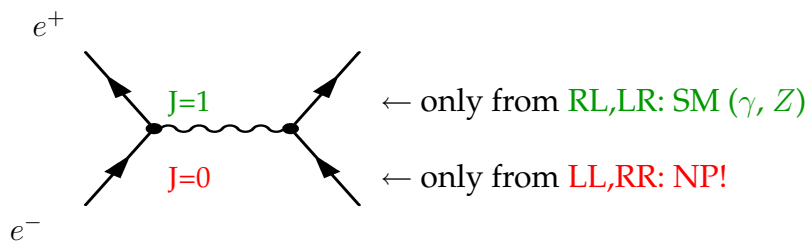
## Introduction

### 1.1 General remarks about the structure of couplings (not complete)

Only some keywords:

Which configurations are possible in principle?

s-channel:



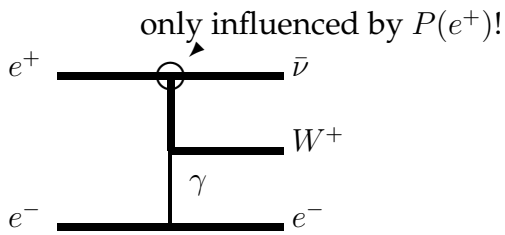
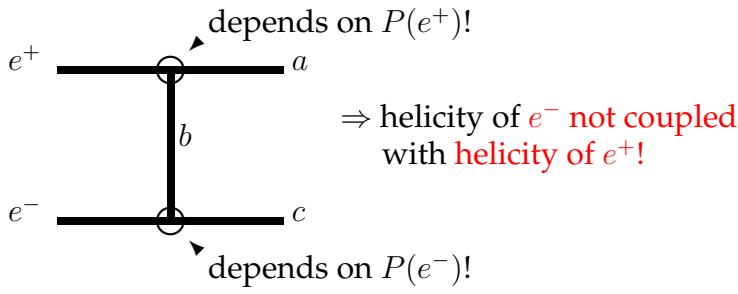
⇒ In principle:  $P(e^-)$  fixes also helicity of  $e^+$ !

Which configurations are possible in the crossed channels?

t-channel:

Two examples:

a) Single  $W$  production



b) Bhabha scattering

$\Rightarrow \gamma, Z$  exchange in s-channel: selects LR, RL  
 $\Rightarrow \gamma, Z$  exchange in t-channel: LL, RR possible

unpolarised	4.50 pb
$P_{e^-} = -80\%$	4.63 pb
$P_{e^-} = -80\%, P_{e^+} = -60\%$	4.69 pb
$P_{e^-} = -80\%, P_{e^+} = +60\%$	4.58 pb

	$e^-$	$e^+$		
$\sigma_{RR}$			$\frac{1+P_{e^-}}{2} \cdot \frac{1+P_{e^+}}{2}$	$J_z = 0$
$\sigma_{LL}$			$\frac{1-P_{e^-}}{2} \cdot \frac{1-P_{e^+}}{2}$	
$\sigma_{RL}$			$\frac{1+P_{e^-}}{2} \cdot \frac{1-P_{e^+}}{2}$	$J_z = 1$
$\sigma_{LR}$			$\frac{1-P_{e^-}}{2} \cdot \frac{1+P_{e^+}}{2}$	

Table 1.1: Graphical representation of the various spin configurations in  $e^+e^-$  collisions. The thick arrow represents the direction of motion of the particle and the double-arrow its spin direction. The first column indicates the corresponding cross section, the third column the fraction of this configuration and the last column the total spin assuming a zero orbital angular momentum.

## 1.2 Longitudinally polarised Electrons (under work)

## 1.3 Improvement of effective Polarisation (not yet final)

In general the cross section of any process in an  $e^+e^-$  collider can be subdivided according to the initial helicity states see 1.1:

$$\sigma = \sigma_{RR} + \sigma_{LL} + \sigma_{RL} + \sigma_{LR}. \quad (1)$$

In the case of  $e^+e^-$  annihilation into a vector particle (in the SM this would be  $e^+e^- \rightarrow \gamma/Z^0$ ) only the two  $J=1$  configurations  $\sigma_{RL}$  and  $\sigma_{LR}$  contribute and the cross section for

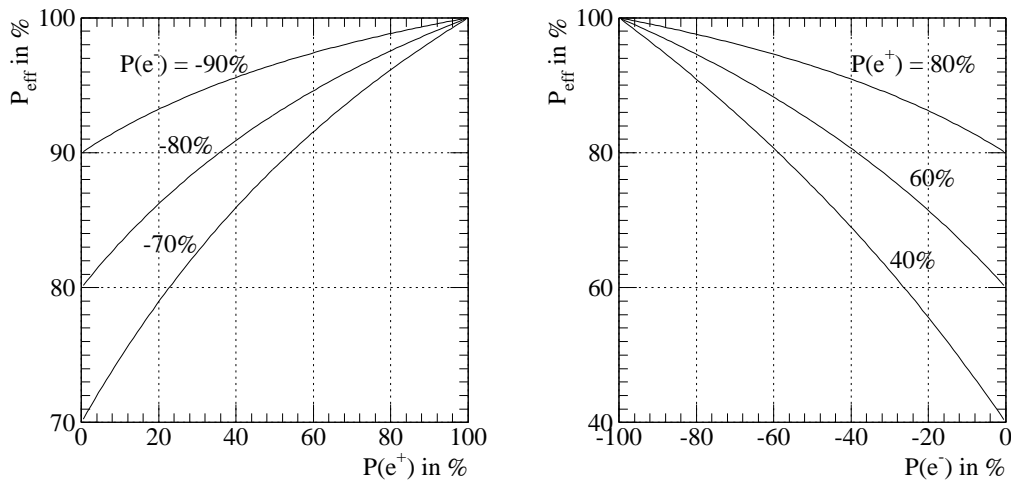


Figure 1: Effective polarization as a function of the beam polarization.

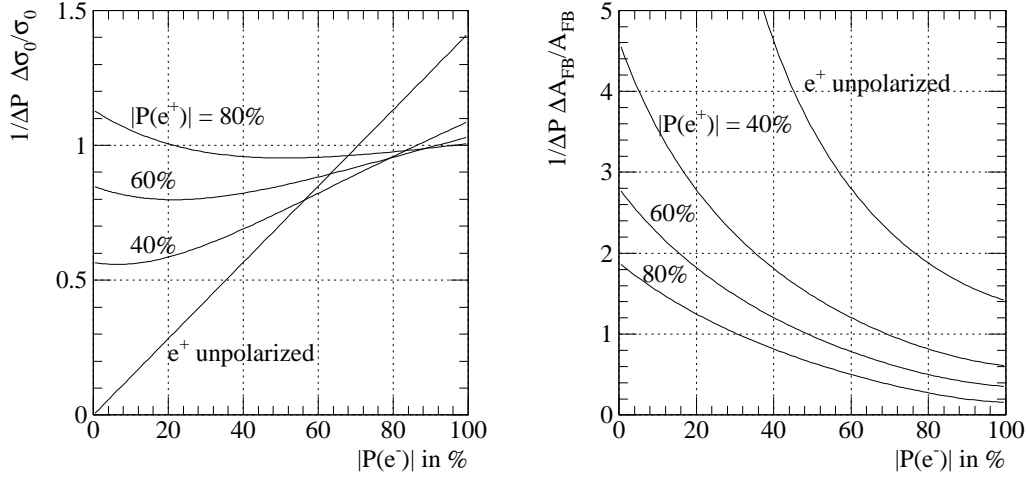


Figure 2: Left: Contribution of the uncertainty on beam polarization on the measurement of the unpolarized cross section. Right: Same for the left-right asymmetry. Both plots are normalized to the polarimeter resolution  $\Delta P$  which is assumed to be identical for both beams.

arbitrary beam polarizations is given by

$$\begin{aligned}
\sigma &= \frac{1 + P_{e^-}}{2} \frac{1 - P_{e^+}}{2} \sigma_{\text{RL}} + \frac{1 - P_{e^-}}{2} \frac{1 + P_{e^+}}{2} \sigma_{\text{LR}} \\
&= (1 - P_{e^-} P_{e^+}) \frac{\sigma_{\text{RL}} + \sigma_{\text{LR}}}{4} \left[ 1 + \frac{P_{e^+} - P_{e^-}}{1 - P_{e^+} P_{e^-}} \frac{\sigma_{\text{LR}} - \sigma_{\text{RL}}}{\sigma_{\text{LR}} + \sigma_{\text{RL}}} \right] \\
&= (1 - P_{e^+} P_{e^-}) \sigma_0 [1 + P_{\text{eff}} A_{\text{LR}}]
\end{aligned} \tag{2}$$

$$\text{with the unpolarized cross section} \quad \sigma_0 = \frac{\sigma_{\text{RL}} + \sigma_{\text{LR}}}{4} \tag{3}$$

$$\text{the left-right asymmetry} \quad A_{\text{LR}} = \frac{\sigma_{\text{LR}} - \sigma_{\text{RL}}}{\sigma_{\text{LR}} + \sigma_{\text{RL}}} \tag{4}$$

$$\text{and the effective polarization} \quad P_{\text{eff}} = \frac{P_{e^+} - P_{e^-}}{1 - P_{e^+} P_{e^-}} \tag{5}$$

The values of the effective polarization can be read from fig. 1. Notice that the effective polarization is closer to 100 % than any of the two beam polarizations. Further excellent reference see also [14].

In the experiment one would like to extract the two quantities  $\sigma_0$  and  $A_{\text{LR}}$ . This can be done by running the experiment with two different polarizations. One would choose one setup with the electron beam predominantly left-handed and the positron beam right-handed and in the second setup one would reverse both spin directions. The cross sections measured with the two setups are denoted as  $\sigma_{-+}$  and  $\sigma_{+-}$ . It is then

$$\begin{aligned}
\sigma_0 &= (1 + |P_{e^+}| |P_{e^-}|) \frac{\sigma_{-+} + \sigma_{+-}}{2} \\
A_{\text{LR}} &= \frac{1}{|P_{\text{eff}}|} \frac{\sigma_{-+} - \sigma_{+-}}{\sigma_{-+} + \sigma_{+-}}
\end{aligned} \tag{6}$$

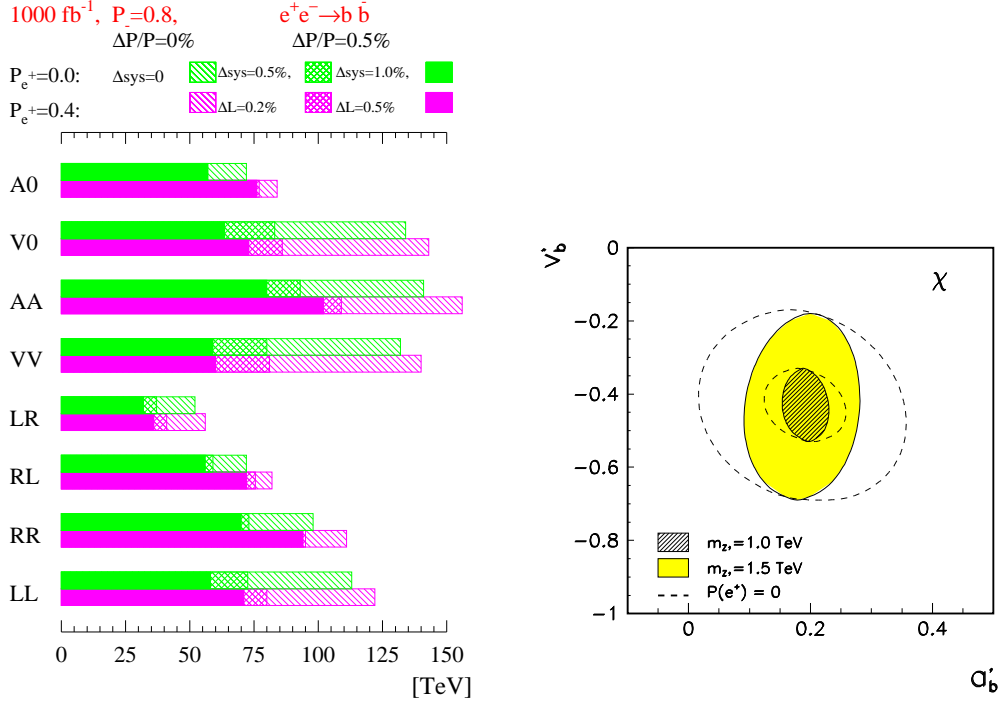


Figure 3: Left: Limits on contact interactions from  $e^+e^- \rightarrow b\bar{b}$  without positron polarization (upper bars) and with 40 % polarization [15]. Right: Accuracy of the  $Z'$  couplings in  $e^+e^- \rightarrow b\bar{b}$  without positron polarization (dashed line) and with 60 % polarization [16].

Both quantities depend on the beam polarizations. The contribution of the uncertainty of the polarization measurement to the error is

$$\begin{aligned} \frac{\Delta\sigma_0}{\sigma_0} &= \frac{\sqrt{2} \Delta P}{1 + |P_{e^+}| |P_{e^-}|} \sqrt{|P_{e^+}|^2 + |P_{e^-}|^2} \\ \frac{\Delta A_{LR}}{A_{LR}} &= -\frac{\Delta P_{\text{eff}}}{|P_{\text{eff}}|} \end{aligned} \quad (7)$$

with

$$\frac{\Delta P_{\text{eff}}}{|P_{\text{eff}}|} = \frac{\sqrt{2} \Delta P}{(|P_{e^+}| + |P_{e^-}|) (1 + |P_{e^+}| |P_{e^-}|)} \sqrt{(1 - |P_{e^-}|^2)^2 + (1 - |P_{e^+}|^2)^2} \quad (8)$$

Equal precision  $\Delta P$  for the measurement of the two beam polarizations is assumed.

The resulting uncertainties are shown in fig. 2. The error contribution from the polarimeter to the unpolarized cross section is rather small. For a polarimeter precision of 0.05 %, it only becomes relevant for data samples with more than  $4 \cdot 10^6$  signal events. For an electron beam polarization of 80 % there is a small improvement in the extraction of the unpolarized cross section due to positron beam polarization.

The error introduced in  $A_{LR}$  by the polarization measurement is larger. Without positron beam polarization one is limited by the polarimeter (0.05 % precision) for samples with more than  $10^6$  events. The improvement due to positron beam polarization is substantial. For a positron polarization of 60 % the error on  $A_{LR}$  is reduced by a factor of 3.8.

In fig. 3 we show an example of the improvements that can be achieved with positron polarization. The left figure shows the achievable limits on contact interactions in  $e^+e^- \rightarrow b\bar{b}$  from the measurements of the cross section,  $A_{LR}$ ,  $A_{FB}$ , and  $A_{FB}^{pol}$  at a center-of-mass energy of 800 GeV [15]. The different pairs of bars show contact interactions with different helicity structures. For each pair the upper bar shows the achievable limits without positron polarization and the lower with a positron polarization of 40 %.

Once new physics is detected positron polarization is even more important to understand the nature of the new interaction. The right plot of fig. 3 shows the accuracy with which the couplings of a new vector boson  $Z'$  could be measured in  $e^+e^- \rightarrow b\bar{b}$  (observables as above, center-of-mass energy 500 GeV). The dashed line indicates the achievable precision without positron polarization for two different  $Z'$  masses while the solid lines assume 60 % positron polarization.

# Chapter 2

## Physics with Polarisation of $e^-$ and $e^+$ beam

### 2.1 Determination of quantum numbers of new physics particles

We demonstrate the determination of quantum numbers at one example of physics beyond the SM: Supersymmetry is one of the most motivated possibilities for NP. However, even its minimal version, the MSSM, leads to about 105 new free parameters. At the LC one has to determine the Susy parameters as model independent as possible, as well as to prove the underlying Susy assumptions, e.g. that the Susy particles have to carry the same quantum numbers (with the exception of the spin) as their SM partners.

E.g. Susy transformations associate chiral (anti)fermions to scalars  $e_{L,R}^- \leftrightarrow \tilde{e}_{L,R}^-$  but  $e_{L,R}^+ \leftrightarrow \tilde{e}_{R,L}^+$ . In order to prove this association the use of both beam polarized is necessary [2]. The process  $e^+e^- \rightarrow \tilde{e}^+\tilde{e}^-$  occurs via  $\gamma$  and  $Z$  exchange in the s-channel and via neutralino  $\tilde{\chi}_i^0$  exchange in the t-channel. The association can be directly tested only in the t-channel and the use of polarized beams serves to separate this channel. We demonstrate this by isolation of the pair  $\tilde{e}_R^+\tilde{e}_L^-$  by the  $LL$  configuration of the initial beams in an example where the selectron masses are close together,  $m_{\tilde{e}_L} = 200$  GeV,  $m_{\tilde{e}_R} = 190$  GeV, so that  $\tilde{e}_L, \tilde{e}_R$  decay via the same decay channels, see Fig. 1a. The other Susy parameters are taken from the reference scenario SPS1a [1]. With  $P_{e^-} = -80\%$ ,  $P_{e^+} = 0\%$  the pairs  $\sigma(\tilde{e}_R^+\tilde{e}_L^-) = 102$  fb and  $\sigma(\tilde{e}_L^+\tilde{e}_L^-) = 108$  fb are close together. This will nearly not be changed even if  $P_{e^-} = -100\%$  were available, which would result in  $\sigma(\tilde{e}_R^+\tilde{e}_L^-) = 113$  fb and  $\sigma(\tilde{e}_L^+\tilde{e}_L^-) = 119$  fb!

However, if we use polarized positrons a separation of the wanted pair  $\tilde{e}_R^+\tilde{e}_L^-$  with the test of the chiral quantum number might be possible:  $P_{e^-} = -80\%$ ,  $P_{e^+} = -40\%$  result in  $\sigma(\tilde{e}_R^+\tilde{e}_L^-) = 143$  fb and  $\sigma(\tilde{e}_L^+\tilde{e}_L^-) = 66$  fb and with  $P_{e^-} = -80\%$ ,  $P_{e^+} = -60\%$  even  $\sigma(\tilde{e}_R^+\tilde{e}_L^-) = 163$  fb,  $\sigma(\tilde{e}_R^+\tilde{e}_R^-) = 49$  fb and  $\sigma(\tilde{e}_L^+\tilde{e}_L^-) = 44$  fb are obtained, see Fig. 1.

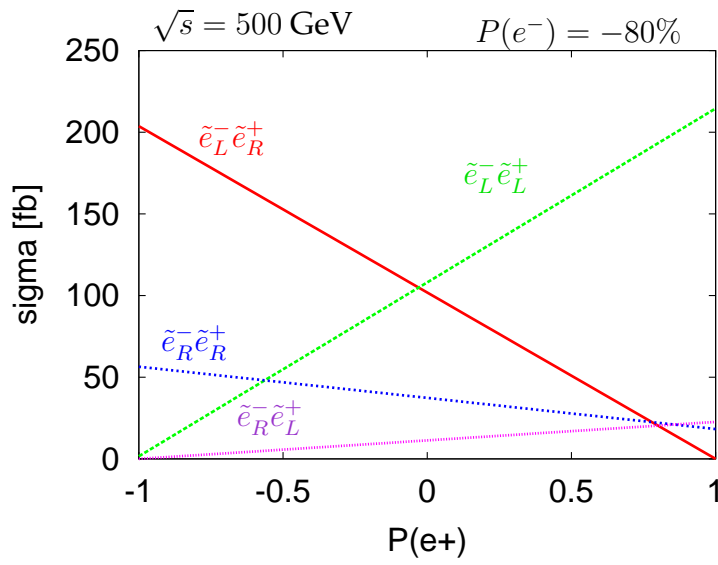


Figure 1: a) Separation of the selectron pair  $\tilde{e}_L^- \tilde{e}_R^+$  in  $e^+e^- \rightarrow \tilde{e}_{L,R}^+ \tilde{e}_{L,R}^-$  with longitudinally polarized beams in order to test the association of chiral quantum numbers to scalar fermions in Susy transformations;

## 2.2 Suppression of Background Channels 3 examples (under work)

2.2.1  $e^+e^- \rightarrow W^+W^-$

2.2.2  $e^+e^- \rightarrow \nu\nu\gamma$ : example ED,  $e^+e^- \rightarrow \gamma G$

2.2.3 Susy example: Smuon production, Uriel

## 2.3 Model-independent contact-interaction analysis at LC: role of electron and positron polarizations

Generally, contact interactions (CI) represent an effective expression of a non-standard dynamics characterized by one (or more) new and very large mass scale exchanges, valid in quark and lepton reactions at the “low” energies  $\sqrt{s} \ll \Lambda$  attainable by current and, perhaps, future accelerators. In this case, the new interactions and dynamical mass scales can manifest themselves only indirectly, through deviations of the measured cross sections from the Standard Model (SM) predictions that, being dimensionally suppressed by some power of  $\sqrt{s}/\Lambda$ , are expected to be quite small. Consequently, high energy reactions in high luminosity and high precision experiments represent a suitable tool to study such signatures. If a deviation is experimentally measured, one can try to identify the effect and the corresponding model. If, conversely, no deviation occurs within the experimental accuracy, one can assess the attainable bounds on the new coupling constants, that are essentially free parameters, by comparing theoretical deviations with experimental statistical and systematic accuracies.

Here, we refer to the fermion pair production process

$$e^+ + e^- \rightarrow f + \bar{f}, \quad (1)$$

with  $f \neq t$ , at an electron-positron Linear Collider (LC) with c.m. energy  $\sqrt{s} = 0.5$  TeV and polarized electron and positron beams, and to the general,  $SU(3) \times SU(2) \times U(1)$  symmetric  $eeff$  dimension  $D = 6$  contact-interaction Lagrangian, with helicity-conserving and flavor-diagonal fermion currents [54]:

$$\mathcal{L}_{\text{CI}} = \frac{1}{1 + \delta_{ef}} \sum_{i,j} g_{\text{eff}}^2 \epsilon_{ij} (\bar{e}_i \gamma_\mu e_i) (\bar{f}_j \gamma^\mu f_j). \quad (2)$$

In Eq. (2):  $i, j = L, R$  denote left- or right-handed helicities, generation and color indices have been suppressed, and the CI coupling constants are parameterized in terms of corresponding mass scales as  $\epsilon_{ij} = \eta_{ij}/\Lambda_{ij}^2$  with  $\eta_{ij} = \pm 1, 0$  depending on the chiral structure of the individual interactions. Also, conventionally  $g_{\text{eff}}^2 = 4\pi$ , as a reminder that, in the case of compositeness, the new interaction would become strong at  $\sqrt{s}$  of the order of  $\Lambda_{ij}$ . Obviously, deviations from the SM and upper bounds or exclusion ranges for the CI couplings can be equivalently expressed as lower bounds and exclusion ranges for the corresponding mass scales  $\Lambda_{ij}$ .

For a given final fermion flavor, apart from the  $\pm$  signs, Eq. (2) envisages four individual, and independent, CI couplings in the case  $f \neq e$  and three couplings in the elastic

$f = e$  case. Correspondingly, the most general (and model-independent) analysis of the process (1) must account for the complicated situation where the full Eq. (2) is included in the expression for the cross section, and all CI couplings can appear there simultaneously as free, non-vanishing, parameters. Although by themselves the helicity amplitudes do not interfere, the numerical constraints on CI couplings can be considerably weakened due to potential cancellations of deviations of helicity amplitudes with opposite signs.

A simplifying procedure is to assume non-zero values for only one of the couplings (or one specific combination of them) at a time with all others set to zero, which would avoid problems associated with negative interference, and leads to tests of *specific* CI models only.

On the other hand, it should be highly desirable to apply a more general kind of experimental data analysis that simultaneously includes all terms of Eq. (2) as independent free parameters and, at the same time, allows the derivation of separate constraints (or exclusion regions) on the individual coupling constants. A strong possibility in this regard is offered by the availability of initial electron and positron longitudinal beam polarizations, that enable to extract from the measured data the individual helicity cross sections  $\sigma_{ij}$  through the definition of particular, and optimal, polarized integrated cross sections and, consequently, to disentangle the constraints on the corresponding CI coupling constants  $\epsilon_{ij}$  [55–57]. Accordingly, a model-independent approach, in the sense stated above, is obtained. Also, it is a well-known fact that, when both the electron and positron beams are polarized, the total annihilation cross section into fermion-antifermion pairs will be increased by a factor [58,59] and, in principle, one could expect a corresponding increase in sensitivity to the new parameters.

## Polarized observables for contact interactions

The analysis of contact-interactions of Ref. [55], that we are briefly summarizing here, is limited to the cases  $f \neq e, t$  where the SM is determined by only  $s$ -channel  $\gamma$  and  $Z$  exchanges and external fermion masses are negligible, and uses as basic observables, to be determined from angular integration of differential rates of events observed with longitudinally polarized beams, the (unpolarized) total cross section  $\sigma_{\text{unpol}}$  and forward-backward asymmetry  $A_{\text{FB}}$ , the left-right asymmetry  $A_{\text{LR}}$  and left-right forward-backward asymmetry  $A_{\text{LR,FB}}$ . These are defined, in the notation of Ref. [60], as:

$$\sigma_{\text{unpol}} = \frac{1}{4} [\sigma_{\text{LL}} + \sigma_{\text{LR}} + \sigma_{\text{RR}} + \sigma_{\text{RL}}], \quad (3)$$

$$A_{\text{FB}} = \frac{3}{4} \frac{\sigma_{\text{LL}} - \sigma_{\text{LR}} + \sigma_{\text{RR}} - \sigma_{\text{RL}}}{\sigma_{\text{LL}} + \sigma_{\text{LR}} + \sigma_{\text{RR}} + \sigma_{\text{RL}}}, \quad (4)$$

$$A_{\text{LR}} = \frac{\sigma_{\text{LL}} + \sigma_{\text{LR}} - \sigma_{\text{RR}} - \sigma_{\text{RL}}}{\sigma_{\text{LL}} + \sigma_{\text{LR}} + \sigma_{\text{RR}} + \sigma_{\text{RL}}}, \quad (5)$$

and

$$A_{\text{LR,FB}} = \frac{3}{4} \frac{\sigma_{\text{LL}} - \sigma_{\text{RR}} + \sigma_{\text{RL}} - \sigma_{\text{LR}}}{\sigma_{\text{LL}} + \sigma_{\text{RR}} + \sigma_{\text{RL}} + \sigma_{\text{LR}}}. \quad (6)$$

The deviations of these observables from the SM predictions are easily expressed in terms of SM couplings and the CI ones,  $\epsilon_{ij}$ , of Eq. (2).

The reach at the LC on the CI couplings, and the corresponding constraints on their allowed values in the case of no indirect effect observed, can be estimated by comparing

the expression of the theoretical deviations determined by the  $\epsilon_{ij}$  with the foreseen experimental (statistical and systematic) uncertainties. The correlation among uncertainties on the four basic observables can be taken into account *via* the method of the covariance matrix [61,62].

As numerical inputs, we assume as reference values the identification efficiencies [63]: 95%, 60% and 35% for the channels for  $l^+l^-$ ,  $b\bar{b}$  and  $c\bar{c}$ , respectively. To assess the relative roles of statistical and systematic uncertainties, we vary the time-integrated luminosity  $\mathcal{L}_{\text{int}}$  from 50 to 500  $\text{fb}^{-1}$  with uncertainty  $\delta\mathcal{L}_{\text{int}}/\mathcal{L}_{\text{int}} = 0.5\%$ , and a fiducial experimental angular range  $|\cos\theta| \leq 0.99$ . Regarding electron and positron degrees of polarization, we consider the values:  $|P_e| = 0.8$ ;  $|P_{\bar{e}}| = 0.0$ , and 0.6, with the uncertainties  $\delta P_e/P_e = \delta P_{\bar{e}}/P_{\bar{e}} = 0.5\%$ .

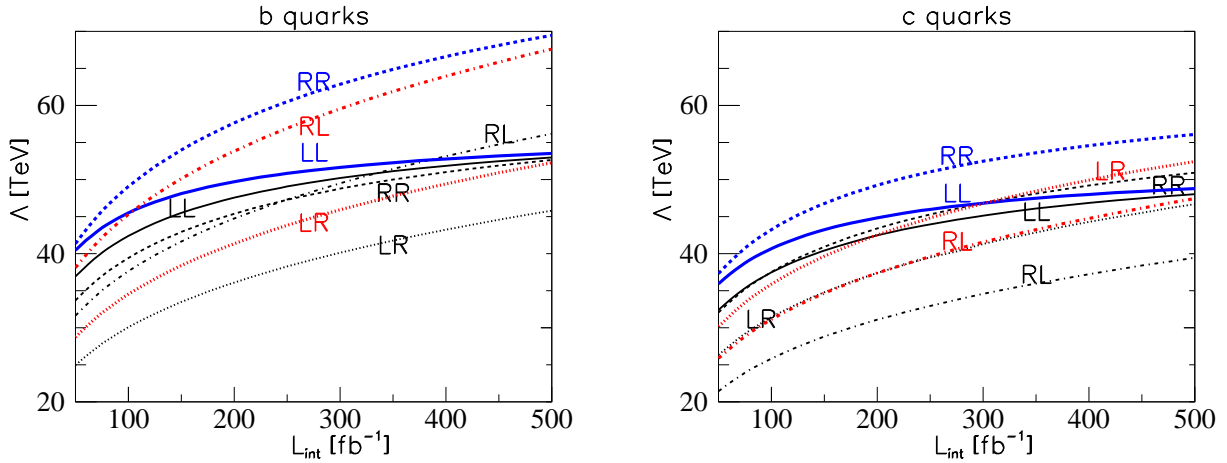


Figure 2: Contact-interaction scale  $\Lambda$  vs. integrated luminosity,  $\mathcal{L}_{\text{int}}$ , for  $b$  and  $c$  quarks, and for the four helicity combinations. Thin curves:  $P_e = 0.8$ ,  $P_{\bar{e}} = 0$ , heavy curves:  $P_e = 0.8$ ,  $P_{\bar{e}} = 0.6$ .

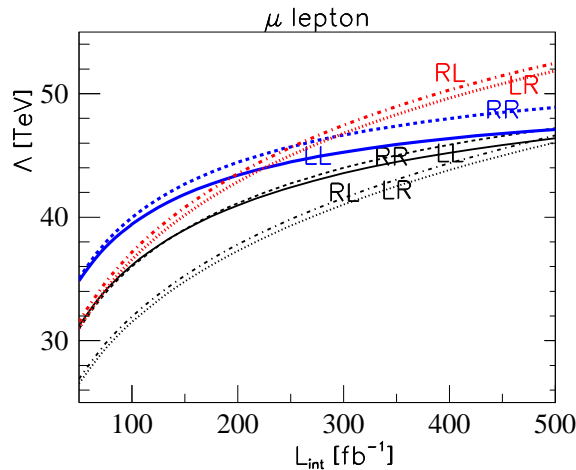


Figure 3: Same as Fig. 2, for muons. (Note other scale.)

The model-independent bounds on the mass scales  $\Lambda_{ij}$  at the 95% C.L. allowed by the experimental uncertainties reported above are shown in Figs. 2 and 3 for the considered

annihilation channels, respectively. In these figures, heavy curves correspond to  $|P_e| = 0.8$ ,  $|P_{\bar{e}}| = 0.6$  while thin curves correspond to  $|P_e| = 0.8$ ,  $|P_{\bar{e}}| = 0.0$ .

As one can see from Eqs. (3) and (4), without simplifying assumptions in the unpolarized case the CI couplings could not be individually constrained within finite ranges, but only mutual correlations could be derived. With initial longitudinal beam polarization, the two additional available physical observables (5) and (6) are essential to obtain finite, model-independent, bounds. In principle, electron beam polarization would be sufficient to achieve this result but, depending on the luminosity and the final  $f\bar{f}$  channel, a significant increase on the sensitivity to CI couplings can arise from the additional availability of positron polarization.

## CI analysis in Bhabha and Møller scattering

With  $\delta_{ef} = 1$  the four-fermion contact interaction Lagrangian of Eq. (2) is relevant to the Bhabha scattering process

$$e^+ + e^- \rightarrow e^+ + e^-, \quad (7)$$

as well as to Møller scattering:

$$e^- + e^- \rightarrow e^- + e^-. \quad (8)$$

The possibility of studying new physics in the process (8) at the LC by turning the positron beam into an electron beam has been considered with interest and, therefore, it should be useful to assess (and compare) the sensitivities of the two processes to the four-electron CI constants of Eq. (2) by a model-independent analysis that simultaneously accounts for all  $\epsilon$ 's as free parameters.

Different from the annihilation processes considered in Sect. 2.3, in the case of processes (7) and (8), apart from the  $\pm$  signs, there are only three (not four) independent CI couplings:  $\epsilon_{LL}$ ,  $\epsilon_{RR}$  and  $\epsilon_{LR} = \epsilon_{RL}$  (same  $\epsilon$ 's for the two processes). The other principal difference, that complicates the procedure to disentangle the constraints on individual couplings, is that Bhabha scattering is determined, in the SM, by  $\gamma$  and  $Z$  exchanges in both the  $s$ - and  $t$ -channels, while Møller scattering is determined by  $\gamma$  and  $Z$  poles in both the  $t$ - and  $u$ -channels.

## Bhabha scattering

With *both* electron and positron beams longitudinally polarized, one can assume that the polarization of each beam can be changed on a pulse by pulse basis, which would allow the separate measurements of the polarized differential cross sections  $d\sigma_{++}$ ,  $d\sigma_{+-}$  and  $d\sigma_{-+}$ , corresponding to the configurations of beam polarizations  $(P_e, P_{\bar{e}}) = (P_1, P_2)$ ,  $(P_1, -P_2)$  and  $(-P_1, P_2)$ , respectively, with  $P_{1,2} > 0$  [64]. They are related to combinations of helicity cross sections  $d\sigma_R$ ,  $d\sigma_L$  and  $d\sigma_{LR,t}$  containing the CI couplings and therefore representing the basic observables for the analysis, by a system of linear equations of the form [64]:

$$\begin{aligned} d\sigma_R &= \frac{(1 + P_2)^2}{2P_2(P_1 + P_2)} d\sigma_{+-} + \frac{(1 - P_1)^2}{2P_1(P_1 + P_2)} d\sigma_{-+} - \frac{1 - P_1P_2}{2P_1P_2} d\sigma_{++}, \\ d\sigma_L &= \frac{(1 - P_2)^2}{2P_2(P_1 + P_2)} d\sigma_{+-} + \frac{(1 + P_1)^2}{2P_1(P_1 + P_2)} d\sigma_{-+} - \frac{1 - P_1P_2}{2P_1P_2} d\sigma_{++}, \end{aligned}$$

$$d\sigma_{\text{LR},t} = -\frac{1-P_2^2}{2P_2(P_1+P_2)}d\sigma_{+-} - \frac{1-P_1^2}{2P_1(P_1+P_2)}d\sigma_{-+} + \frac{1+P_1P_2}{2P_1P_2}d\sigma_{++}. \quad (9)$$

It turns out that, while  $\sigma_{\text{LR},t}$  (that is pure  $t$ -pole) depends on a single contact interaction parameter ( $\epsilon_{\text{LR}}$ ), which therefore can be *directly* disentangled from the other couplings,  $\sigma_{\text{R}}$  and  $\sigma_{\text{L}}$  simultaneously depend on *pairs* of parameters, ( $\epsilon_{\text{RR}}, \epsilon_{\text{LR}}$ ) and ( $\epsilon_{\text{RR}}, \epsilon_{\text{LL}}$ ), respectively, and in this case (ellipsoidal) allowed areas in the relevant planes can be obtained. This clearly shows that *both* electron *and* positron polarization are needed to perform a model-independent analysis of CI couplings in Bhabha scattering. One can easily see that, without polarization ( $P_1 = P_2 = 0$ ), in the general case only correlations among couplings can be derived and, in particular, the contribution of  $\epsilon_{\text{LR}}$  is subject to partial cancellations.

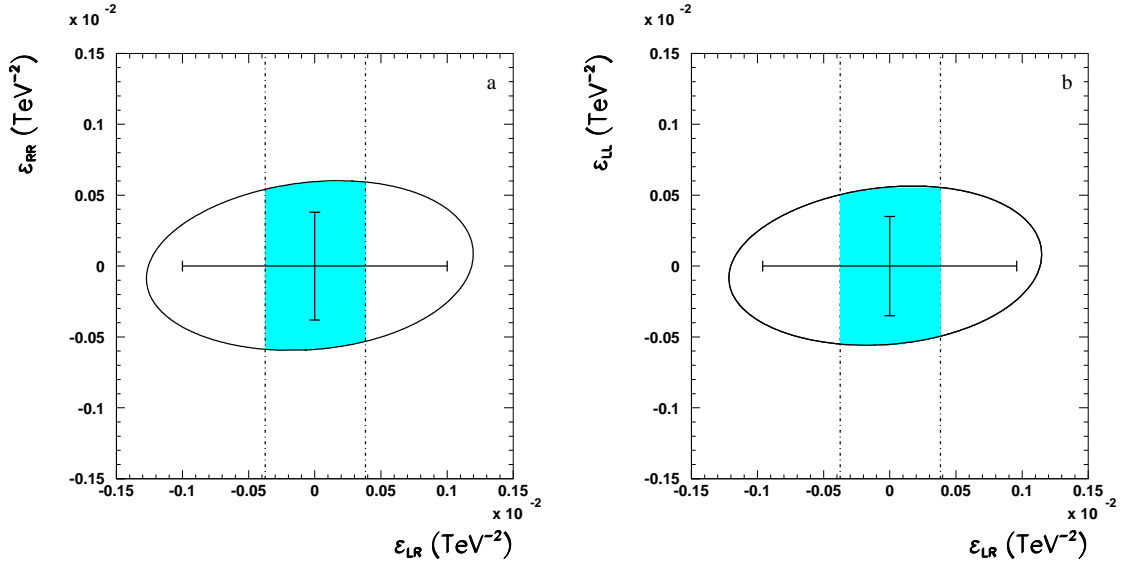


Figure 4: Allowed areas at 95% C.L. in the planes  $(\epsilon_{\text{LR}}, \epsilon_{\text{RR}})$  and  $(\epsilon_{\text{LR}}, \epsilon_{\text{LL}})$  obtained from  $\sigma_{\text{R}}$  and  $\sigma_{\text{L}}$  in  $e^+e^- \rightarrow e^+e^-$  at  $\sqrt{s} = 0.5$  TeV,  $\mathcal{L}_{\text{int}}(e^+e^-) = 50 \text{ fb}^{-1}$ ,  $|P_e| = 0.8$ ,  $|P_{\bar{e}}| = 0.6$ . Vertical dashed lines indicate the range allowed to  $\epsilon_{\text{LR}}$  by  $\sigma_{\text{LR},t}$ .

To assess the sensitivity of Bhabha scattering to the compositeness scale, in Fig. 4 we depict as an example the 95% C.L. contours around  $\epsilon_{\text{LL}} = \epsilon_{\text{RR}} = \epsilon_{\text{LR}}$  in the two-dimensional planes  $(\epsilon_{\text{RR}}, \epsilon_{\text{LR}})$  and  $(\epsilon_{\text{RR}}, \epsilon_{\text{LL}})$ , derived from a  $\chi^2$  analysis of differential cross sections, assuming that no deviation from the SM within the experimental uncertainty (statistical and systematic) is measured in  $d\sigma_{\text{L}}$ ,  $d\sigma_{\text{R}}$  and  $d\sigma_{\text{LR},t}$  ( $\mathcal{L}_{\text{int}}(e^+e^-) = 50 \text{ fb}^{-1}$ ,  $P_1 = 0.8$ ,  $P_2 = 0.6$ ,  $\delta\mathcal{L}_{\text{int}}/\mathcal{L}_{\text{int}} = \delta P_1/P_1 = \delta P_2/P_2 = 0.5\%$ ). The crosses indicate the constraints obtained by taking one non-zero parameter at a time instead of two simultaneously non-zero and independent.

In Fig. 5 we show the maximum reachable values (95% C.L.) on the mass scales  $\Lambda$  as a function of the time-integrated luminosity at the LC. The dramatic sensitivity of process (7) to  $\Lambda_{\text{LR}}$ , that can be disentangled directly owing to polarization, is clearly shown by this figure.

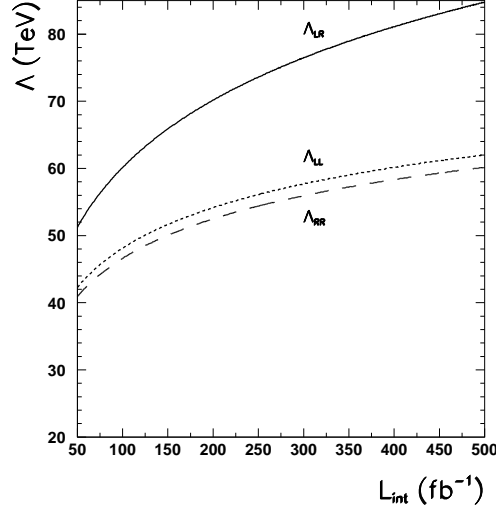


Figure 5: Model-independent reach on  $\Lambda$  at 95% C.L. vs.  $\mathcal{L}_{\text{int}}(e^+e^-)$  from  $e^+e^- \rightarrow e^+e^-$  at  $\sqrt{s} = 0.5$  TeV,  $|P_e| = 0.8$ ,  $|P_{\bar{e}}| = 0.6$ .

## Møller scattering with polarized electrons

Similar to process (7), in this case the SM amplitudes have both  $t$ - and  $u$ -poles. However, there is an outstanding difference: denoting by  $P_e^{(1)}$  and  $P_e^{(2)}$  the degree of initial electron longitudinal polarization, and by  $d\sigma_{++}$ ,  $d\sigma_{--}$  and  $d\sigma_{+-}$  the measurable polarized differential cross sections corresponding to the three configurations  $(P_e^{(1)}, P_e^{(2)}) = (P_1, P_2)$ ,  $(-P_1, -P_2)$  and  $(P_1, -P_2)$ , respectively, with  $P_{1,2} > 0$ , the analogue of the system of linear equations (9) is [64]:

$$\begin{aligned}
d\sigma_{\text{RR}} &= \frac{(1+P_2)^2}{2P_2(P_1+P_2)} d\sigma_{++} + \frac{(1-P_1)^2}{2P_1(P_1+P_2)} d\sigma_{--} - \frac{1-P_1P_2}{2P_1P_2} d\sigma_{+-}, \\
d\sigma_{\text{LL}} &= \frac{(1-P_2)^2}{2P_2(P_1+P_2)} d\sigma_{++} + \frac{(1+P_1)^2}{2P_1(P_1+P_2)} d\sigma_{--} - \frac{1-P_1P_2}{2P_1P_2} d\sigma_{+-}, \\
d\sigma_{\text{LR}} &= -\frac{1-P_2^2}{2P_2(P_1+P_2)} d\sigma_{++} - \frac{1-P_1^2}{2P_1(P_1+P_2)} d\sigma_{--} + \frac{1+P_1P_2}{2P_1P_2} d\sigma_{+-}, \quad (10)
\end{aligned}$$

and each of the cross sections  $\sigma_{\text{RR}}$ ,  $\sigma_{\text{LL}}$  and  $\sigma_{\text{LR}}$  depend on an individual contact-interaction parameter. Therefore, complete disentangling of the various CI couplings (hence the derivation of model-independent constraints) is *directly* achieved in the Møller process with both beams polarized.

In Fig. 6 we report the 95% C.L. model-independent reach on  $\Lambda$ 's vs. the integrated luminosity, that can be attained from process (8) at the LC with  $\sqrt{s} = 0.5$  TeV and both initial electrons longitudinally polarized with  $P_1 = P_2 = 0.8$  (systematic uncertainties are assumed to be the same as in the previous case). As regards the range of values of the luminosity, we have taken into account that  $\mathcal{L}_{\text{int}}(e^-e^-)$  at the linear collider is expected to be somewhat reduced by anti-pinching compared to  $\mathcal{L}_{\text{int}}(e^+e^-)$ , typically by a factor 1/7 to 1/3, which, of course, tends to depress the sensitivity to the new physics. One can see,

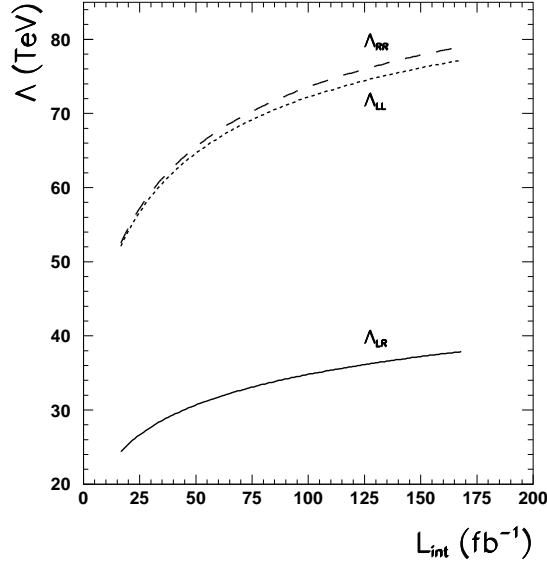


Figure 6: Model-independent reach on  $\Lambda$  at 95% C.L. vs.  $\mathcal{L}_{\text{int}}(e^-e^-)$  from  $e^-e^- \rightarrow e^-e^-$  at  $\sqrt{s} = 0.5$  TeV and  $|P_e^{(1)}| = |P_e^{(2)}| = 0.8$ .

compared to Fig. 5, the higher sensitivity of the polarized process (8) to  $\Lambda_{LL}$  and  $\Lambda_{RR}$  with respect to  $\Lambda_{LR}$ .

One can conclude, finally, as far as the sensitivity to individual couplings in a model-independent data analysis is concerned that, if  $\mathcal{L}_{\text{int}}(e^-e^-)$  is not too low, the two processes (7) and (8) are somehow complementary. Also, the advantage of having both initial beams polarized, that allows the measurement of suitable polarized cross sections in order to disentangle the different contact-interaction couplings, is clear.

## Identification of graviton exchange effects

Process (1) at the LC has been considered with much interest as a tool to look for effects related to large extra dimensions and low-scale gravity [65, 66], in particular the virtual effects from KK graviton exchange. This effect can in the ADD scenario [65] be modeled, in the framework of contact interactions, by the effective Lagrangian [67]

$$\mathcal{L} = i \frac{4\lambda}{M_H^4} T_{\mu\nu} T^{\mu\nu}, \quad (11)$$

where  $T_{\mu\nu}$  is the energy-momentum tensor,  $M_H$  is the relevant graviton cut-off mass scale and  $\lambda$  is a sign factor ( $\lambda = \pm 1$ ). In principle, one could apply the same arguments as outlined in the previous sections to derive the sensitivity to (11) and the corresponding reach on  $M_H$  by considering the deviations from the Standard Model predictions caused by this kind of interaction and numerically comparing them to the foreseen experimental uncertainties on the cross sections. Actually, since there is only one coupling, polarization would not be strictly required, and the only difference that remains would be that, compared to the previous contact-interaction Lagrangian (2), being induced by a dimension  $D = 8$  operator the KK graviton exchange is suppressed by the much higher power

$(\sqrt{s}/M_H)^4$ , so that a lower reach on  $M_H$  can be expected in comparison to the constraints obtainable, at the same c.m. energy, on the  $\Lambda$ 's.

On the other hand, due to its spin-2 character, the deviations produced by KK exchange in the helicity amplitudes of process (1) have a specific angular dependence, whereas those from the interactions represented by (2), due to their vector current-current form, have a different angular dependence. Accordingly, for final  $f\bar{f}$  channels with  $f \neq e$  dominated in the SM by  $s$ -channel  $\gamma$  and  $Z$  exchanges, there is the possibility of uniquely identifying in the data analysis the effects of graviton exchange from other new physics.

In this connection, a particularly suitable observable is represented by the generalized centre-edge asymmetry among integrated differential distributions [68]:

$$A_{\text{CE}} = \frac{\sigma_{\text{CE}}}{\sigma}, \quad (12)$$

with

$$\sigma_{\text{CE}} = \left[ \int_{-z^*}^{z^*} - \left( \int_{-1}^{-z^*} + \int_{z^*}^1 \right) \right] \frac{d\sigma}{dz} dz, \quad \sigma = \int_{-1}^1 \frac{d\sigma}{dz} dz \quad (13)$$

and  $0 < z^* < 1$  (here,  $z = \cos \theta$  with  $\theta$  the angle between electron and outgoing fermion in the c.m.).

A crucial feature of  $A_{\text{CE}}$  is that it is *identical* to that of the SM even if contact-interaction-like interactions are present:

$$A_{\text{CE}}^{\text{SM+CI}} \equiv A_{\text{CE}}^{\text{SM}} = \frac{1}{2} z^* (z^{*2} + 3) - 1, \quad (14)$$

independent of final-state flavour, energy, and longitudinal beam polarization and therefore, for these interactions, there is no deviation. Conversely,  $A_{\text{CE}}$  with graviton exchange is *different* and *does* depend on final state flavor and initial beam polarization, and the largest deviation  $\Delta A_{\text{CE}}$  from  $A_{\text{CE}}^{\text{SM}}$  is produced by the interference of the SM with Eq. (11). Therefore, the asymmetry (12) has the property of “filtering out” the “conventional” contact interactions represented by the Lagrangian (2) from deviations from the SM, and consequently of providing a clear signature for graviton exchange, particularly for choices of  $z^*$  around the value  $z_0^* = 0.596$  where the right-hand side of (14) vanishes and the effect (hence, the sensitivity) is maximal.

In Fig. 7 we present, as an example, the  $5\sigma$  identification reach on the mass scale  $M_H$ , summing over the channels  $f = \mu, \tau, b, c$ , that can be obtained at the LC by a  $\chi^2$  analysis assuming that no deviation  $\Delta A_{\text{CE}}$  is seen within the experimental accuracy, with the same assumptions on the integrated luminosity and the initial beam polarization (and the corresponding uncertainties) considered previously. Thin, medium and heavy curves refer, respectively, to the cases  $(P_e = P_{\bar{e}} = 0)$ ,  $(P_e = 0.8, P_{\bar{e}} = 0)$  and  $(P_e = 0.8, P_{\bar{e}} = 0.6)$ .

Longitudinal beam polarization appears to increase the sensitivity to graviton exchange, although the impact on  $M_H$  is less dramatic in this case due to the suppression  $(\sqrt{s}/M_H)^4$  of the graviton coupling. Instead, initial polarization can be seen to play a key role in distinguishing graviton exchange from competing effects, such as those originating from scalar particle exchange in both  $s$ - and  $t$ -channels, that can be “filtered” out by appropriate polarization asymmetries [68,69].

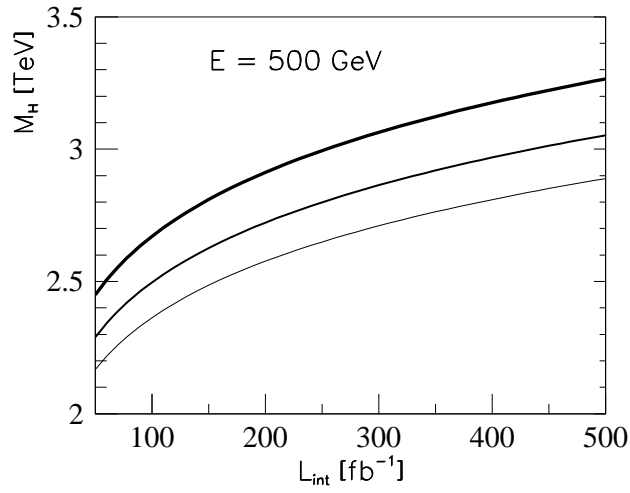


Figure 7:  $5\sigma$  reach on the mass scale  $M_H$  vs. integrated luminosity from the process  $e^+e^- \rightarrow f\bar{f}$ , with  $f$  summed over  $\mu, \tau, b, c$ , and for the energy 0.5 TeV. Thin: unpolarized; medium: electrons polarized,  $P_e = 0.8$ ; heavy: both beams polarized,  $P_e = 0.8$ ,  $P_{\bar{e}} = -0.6$ .

## 2.4 Determination of sfermion parameters

The search for supersymmetric (SUSY) particles will be one of the main goals of a future  $e^+e^-$  linear collider with an energy range  $\sqrt{s} = 0.5 - 1$  TeV [46]. Such an  $e^+e^-$  linear collider will also be very well suited for the precision determination of the parameters of the underlying SUSY model, in particular if polarized beams are available. The precise determination will be necessary to determine the mechanisms of SUSY breaking and electroweak symmetry breaking and eventually to reconstruct of the underlying high scale theory [47].

In this contribution we summarize the results of our recent phenomenological studies on the production of third generation sfermions in  $e^+e^-$  annihilation at  $\sqrt{s} = 500$  GeV [48]. We take into account the effects of both  $e^-$  and  $e^+$  beam polarizations. The main advantages of using polarized beams are: (i) larger cross sections can be obtained, (ii) background reactions can be suppressed, (iii) measurements of appropriate observables lead to additional information on the SUSY parameters. All calculations are performed within the Minimal Supersymmetric Standard Model (MSSM) with real parameters.

### Sfermion Production

In the third generation, Yukawa terms give rise to mixing between the ‘left’ and ‘right’ states  $\tilde{f}_L$  and  $\tilde{f}_R$  ( $\tilde{f} = \tilde{t}, \tilde{b}, \tilde{\tau}$ ). Neglecting the mixing between generations this mixing is described by a hermitian  $2 \times 2$  mass matrix which depends on the soft SUSY-breaking mass parameters  $M_{\tilde{Q}}, M_{\tilde{U}}$  etc., and the trilinear scalar coupling parameters  $A_t, A_b, A_\tau$ . The mass eigenstates are  $\tilde{f}_1 = \tilde{f}_L \cos \theta_{\tilde{f}} + \tilde{f}_R \sin \theta_{\tilde{f}}$ , and  $\tilde{f}_2 = \tilde{f}_R \cos \theta_{\tilde{f}} - \tilde{f}_L \sin \theta_{\tilde{f}}$ , with  $\theta_{\tilde{f}}$  the sfermion mixing angle. Information on the sfermion mixing angle can be obtained from measuring production cross sections using different combinations of beam polarizations as we discuss below taking the production of light stops as a particular example.

The reaction  $e^+e^- \rightarrow \tilde{f}_i \tilde{f}_j$  proceeds via  $\gamma$  and  $Z$  exchange in the  $s$ -channel. The  $\tilde{f}_i$  couplings depend on the sfermion mixing angle  $\theta_{\tilde{f}}$ . In Figs. 8 a, b we show contour lines of the cross section  $\sigma(e^+e^- \rightarrow \tilde{t}_1 \tilde{t}_1)$  as a function of the  $e^-$  and  $e^+$  beam polarizations  $\mathcal{P}_-$  and  $\mathcal{P}_+$  at  $\sqrt{s} = 500$  GeV for  $m_{\tilde{t}_1} = 200$  GeV and (a)  $\cos \theta_{\tilde{t}} = 0.4$  and (b)  $\cos \theta_{\tilde{t}} = 0.66$ . We have included initial-state radiation (ISR) and SUSY-QCD corrections (for details see [48, 49]). The white windows show the range of polarizations  $|\mathcal{P}_-| < 0.9$  and  $|\mathcal{P}_+| < 0.6$ . As can be seen, one can significantly increase the cross section by using the highest possible  $e^-$  and  $e^+$  polarization available. Moreover, beam polarization strengthens the  $\cos \theta_{\tilde{t}}$  dependence and can thus be essential for determining the mixing angle. Corresponding cross sections for the production of sbottoms, staus and  $\tau$ -sneutrinos are presented in [48].

### Parameter Determination

We estimate the precision one may obtain for the parameters of the  $\tilde{t}$  sector from cross section measurements using the parameter point  $m_{\tilde{t}_1} = 200$  GeV,  $\cos \theta_{\tilde{t}} = -0.66$  as an illustrative example: For  $\mathcal{P}_- = -0.9$  we find  $\sigma_L(\tilde{t}_1 \tilde{t}_1) = 44.88$  fb and for  $\mathcal{P}_- = 0.9$   $\sigma_R(\tilde{t}_1 \tilde{t}_1) = 26.95$  fb (with  $\mathcal{P}_+ = 0$ ) including SUSY-QCD, Yukawa coupling, and ISR corrections. According to the Monte Carlo study of [50] one can expect to measure the  $\tilde{t}_1 \tilde{t}_1$  production cross sections with a statistical error of  $\Delta\sigma_L/\sigma_L = 2.1\%$  and  $\Delta\sigma_R/\sigma_R = 2.8\%$

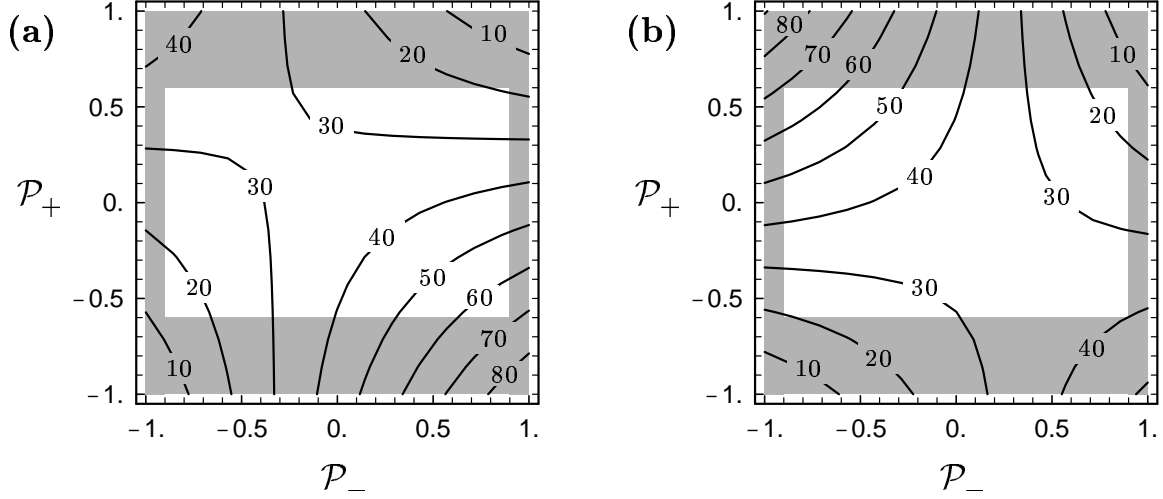


Figure 8: Dependence of  $\sigma(e^+e^- \rightarrow \tilde{t}_1\tilde{t}_1)$  on degree of electron and positron polarization at  $\sqrt{s} = 500$  GeV, for  $m_{\tilde{t}_1} = 200$  GeV,  $\cos\theta_{\tilde{t}} = 0.4$  in (a) and  $\cos\theta_{\tilde{t}} = 0.66$  in (b).

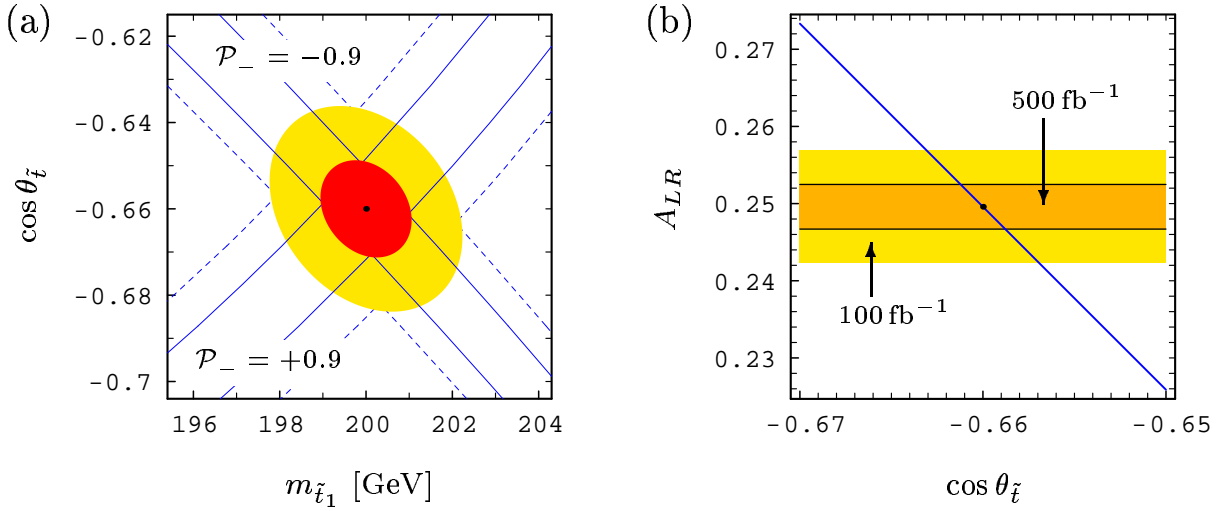


Figure 9: (a) Error bands and 68% CL error ellipse for determining  $m_{\tilde{t}_1}$  and  $\cos\theta_{\tilde{t}}$  from cross section measurements; the dashed lines are for  $\mathcal{L} = 100$  fb $^{-1}$  and the full lines for  $\mathcal{L} = 500$  fb $^{-1}$ . (b) Error bands for the determination of  $\cos\theta_{\tilde{t}}$  from  $A_{LR}$ . In both plots  $m_{\tilde{t}_1} = 200$  GeV,  $\cos\theta_{\tilde{t}} = -0.66$ ,  $\sqrt{s} = 500$  GeV,  $\mathcal{P}_- = \pm 0.9$ ,  $\mathcal{P}_+ = 0$ .

in case of an integrated luminosity of  $\mathcal{L} = 500$  fb $^{-1}$  (i.e.  $\mathcal{L} = 250$  fb $^{-1}$  for each polarization). Scaling these values to  $\mathcal{L} = 100$  fb $^{-1}$  leads to  $\Delta\sigma_L/\sigma_L = 4.7\%$  and  $\Delta\sigma_R/\sigma_R = 6.3\%$ . Figure 9 a shows the corresponding error bands and error ellipses in the  $m_{\tilde{t}_1} - \cos\theta_{\tilde{t}}$  plane. The resulting errors on the stop mass and mixing angle are:  $\Delta m_{\tilde{t}_1} = 2.2$  GeV,  $\Delta \cos\theta_{\tilde{t}} = 0.02$  ( $\Delta m_{\tilde{t}_1} = 1.1$  GeV,  $\Delta \cos\theta_{\tilde{t}} = 0.01$ ) for  $\mathcal{L} = 100$  fb $^{-1}$  ( $\mathcal{L} = 500$  fb $^{-1}$ ). If in addition the  $e^+$  beam is 60% polarized these values can be improved by  $\sim 25\%$ .

For the determination of the mixing angle, one can also make use of the left-right asymmetry  $A_{LR} \equiv [\sigma(-|\mathcal{P}_-|, |\mathcal{P}_+|) - \sigma(|\mathcal{P}_-|, -|\mathcal{P}_+|)] / [\sigma(-|\mathcal{P}_-|, |\mathcal{P}_+|) + \sigma(|\mathcal{P}_-|, -|\mathcal{P}_+|)]$ . We get  $A_{LR}(e^+e^- \rightarrow \tilde{t}_1\tilde{t}_1) = 0.2496$  for  $m_{\tilde{t}_1} = 200$  GeV,  $\cos\theta_{\tilde{t}} = -0.66$ ,  $\sqrt{s} = 500$  GeV,  $\mathcal{P}_- = 0.9$ , and  $\mathcal{P}_+ = 0$ . Taking into account experimental errors as determined in [50], a theoretical uncertainty of 1%, and  $\Delta P/P = 10^{-2}$  we get  $\Delta A_{LR} = 2.92\%$  (1.16%) for

$\mathcal{L} = 100 \text{ fb}^{-1}$  ( $500 \text{ fb}^{-1}$ ). This corresponds to  $\Delta \cos \theta_{\tilde{t}} = 0.0031$  ( $0.0012$ ). This is most likely the most precise method to determine the stop mixing angle. The corresponding error bands are shown in Fig. 9 b.

Once produced, sfermions will decay into e.g.,  $\tilde{t}_1 \rightarrow b\tilde{\chi}_1^+$ ,  $\tilde{b}_1 \rightarrow b\tilde{\chi}_1^0$ ,  $\tilde{\tau}_1 \rightarrow \tau\tilde{\chi}_1^0$ , etc. Information on the polarization of the fermions in the final states can be used to further improve the precision on the SUSY parameters [51,52]. The basic SUSY breaking parameters of the sfermion mass matrix can be extracted if both masses and the mixing angle are known. In particular,  $A_t$  is given by  $A_t = \mu \cot \beta + (m_{\tilde{t}_1}^2 - m_{\tilde{t}_2}^2) \sin 2\theta_{\tilde{t}} / (2m_t)$ , and likewise for  $A_b$  and  $A_\tau$  where  $\cot \beta$  has to be replaced by  $\tan \beta$ . The precise determination of these parameters is in particular important for reconstruction of the high scale theory and for the determination of the SUSY breaking mechanism [47]. Moreover, it allows for cross checks with the determination of  $A_t$  from the Higgs sector [53].

## 2.5 Sfermion Mass measurements in the continuum (will be written by Uriel)

## 2.6 CP asymmetries in Neutralino Production and 2-body decay

In the neutralino sector of the Minimal Supersymmetric Standard Model (MSSM) [32], the gaugino mass parameter  $M_1$ , the higgsino mass parameter  $\mu$ , and the trilinear coupling parameter  $A_\tau$  in the stau sector, can be complex. The physical phases  $\varphi_{M_1}$ ,  $\varphi_\mu$  and  $\varphi_{A_\tau}$  of these parameters can cause large CP-violating effects already at tree level.

In neutralino production

$$e^- + e^+ \rightarrow \tilde{\chi}_i^0 + \tilde{\chi}_j^0 \quad (15)$$

and the subsequent leptonic two-body decay of one of the neutralinos

$$\tilde{\chi}_i^0 \rightarrow \tilde{\ell} + l_1, \quad (16)$$

and of the decay slepton

$$\tilde{\ell} \rightarrow \tilde{\chi}_1^0 + l_2; \quad l_{1,2} = e, \mu, \tau, \quad (17)$$

the neutralino spin correlations lead to several CP-odd asymmetries. With the triple product  $\mathcal{T} = (\vec{p}_{e^-} \times \vec{p}_{\ell_2}) \cdot \vec{p}_{\ell_1}$ , we define the *T-odd* asymmetry of the cross section  $\sigma$  for the processes (15)-(17):

$$\mathcal{A}_T = \frac{\sigma(\mathcal{T} > 0) - \sigma(\mathcal{T} < 0)}{\sigma(\mathcal{T} > 0) + \sigma(\mathcal{T} < 0)}. \quad (18)$$

If absorptive phases are neglected,  $\mathcal{A}_T$  is CP-odd due to CPT invariance. The dependence of  $\mathcal{A}_T$  on  $\varphi_{M_1}$  and  $\varphi_\mu$  was analyzed in [33–35].

In case the neutralino decays into a  $\tau$ -lepton,  $\tilde{\chi}_i^0 \rightarrow \tilde{\tau}_k^\pm \tau^\mp$ ,  $k = 1, 2$ , the T-odd transverse  $\tau^-$  and  $\tau^+$  polarizations  $P_2$  and  $\bar{P}_2$ , respectively, give rise to the *CP-odd* observable

$$\mathcal{A}_{CP} = \frac{1}{2}(P_2 - \bar{P}_2), \quad (19)$$

which is also sensitive to  $\varphi_{A_\tau}$ . For various MSSM scenarios,  $\mathcal{A}_{CP}$  was discussed in [36]. For measuring the asymmetries, it is crucial to have both large asymmetries and large cross sections. In this note we study the impact of longitudinally polarized  $e^+$  and  $e^-$  beams of a future linear collider in the 500 GeV range on the asymmetries  $\mathcal{A}_T$ ,  $\mathcal{A}_{CP}$  and on the cross sections  $\sigma$ .

## Numerical results

We present numerical results for  $e^+e^- \rightarrow \tilde{\chi}_1^0\tilde{\chi}_2^0$  with the subsequent leptonic decay of  $\tilde{\chi}_2^0$  for a linear collider with  $\sqrt{s} = 500$  GeV. For  $\mathcal{A}_T$ , Eq. (18), we study the neutralino decay into the right selectron and right smuon,  $\tilde{\chi}_2^0 \rightarrow \tilde{\ell}_R l_1$ ,  $\ell = e, \mu$  and for  $\mathcal{A}_{CP}$ , Eq. (19), that

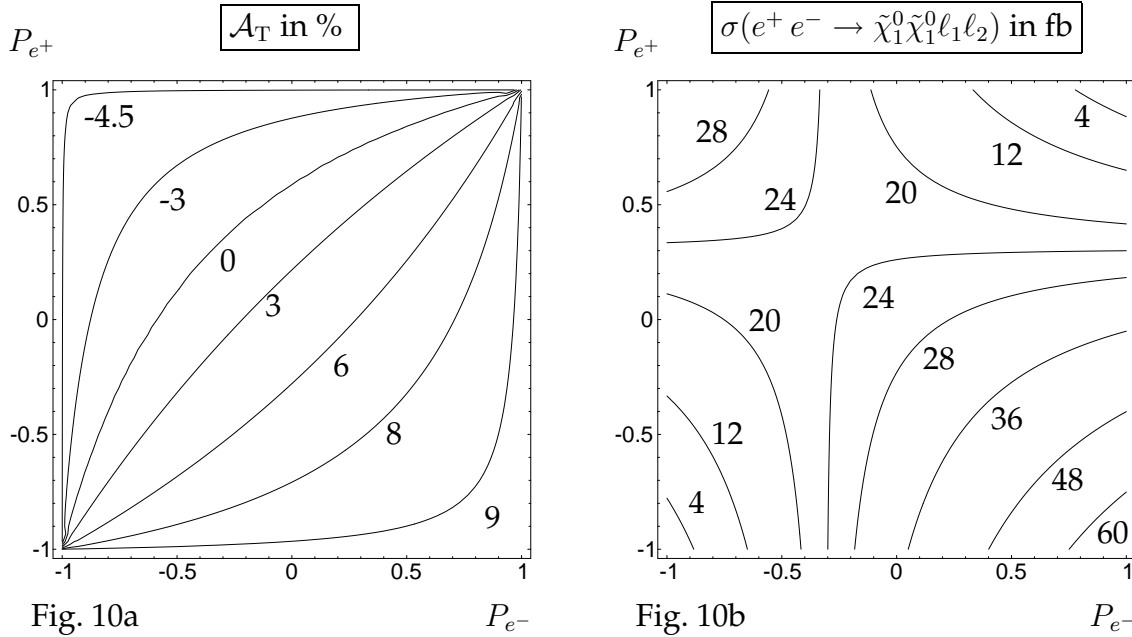


Figure 10: Contour lines of  $\mathcal{A}_T$  and  $\sigma$  for  $\varphi_{M_1} = 0.2\pi$ ,  $\varphi_\mu = 0$ ,  $|\mu| = 240$  GeV,  $M_2 = 400$  GeV,  $\tan\beta = 10$  and  $m_0 = 100$  GeV.

into the lightest scalar tau,  $\tilde{\chi}_2^0 \rightarrow \tilde{\tau}_1 \tau$ . We study the dependence of the asymmetries and the cross sections on the beam polarizations  $P_{e^-}$  and  $P_{e^+}$  for fixed parameters  $\mu = |\mu| e^{i\varphi_\mu}$ ,  $M_1 = |M_1| e^{i\varphi_{M_1}}$ ,  $A_\tau = |A_\tau| e^{i\varphi_{A_\tau}}$ ,  $M_2$  and  $\tan\beta$ . We assume  $|M_1| = 5/3 M_2 \tan^2 \theta_W$  and use the renormalization group equations [37] for the selectron and smuon masses,  $m_{\tilde{\ell}_R}^2 = m_0^2 + 0.23 M_2^2 - m_Z^2 \cos 2\beta \sin^2 \theta_W$  with  $m_0 = 100$  GeV. The interaction Lagrangians and details on stau mixing can be found in [35].

In Fig. 10a we show the dependence of  $\mathcal{A}_T$  on the beam polarization for  $\varphi_{M_1} = 0.2\pi$  and  $\varphi_{A_\tau} = \varphi_\mu = 0$ . A small value of  $\varphi_\mu$  is suggested by constraints on electron and neutron electric dipole moments (EDMs) [38] for a typical SUSY scale of the order of a few 100 GeV (for a review see, e.g., [39]). It is remarkable that in our scenario the asymmetry can be close to 10% even for the small value of  $\varphi_{M_1} = 0.2\pi$  and for  $\varphi_\mu = 0$ . The cross section  $\sigma = \sigma(e^+ e^- \rightarrow \tilde{\chi}_1^0 \tilde{\chi}_2^0) \times \text{BR}(\tilde{\chi}_2^0 \rightarrow \tilde{\ell}_R \ell_1) \times \text{BR}(\tilde{\ell}_R \rightarrow \tilde{\chi}_1^0 \ell_2)$  is shown in Fig. 10b. For our scenario with  $|A_\tau| = 250$  GeV and  $\varphi_{A_\tau} = 0$ , the neutralino branching ratio is  $\text{BR}(\tilde{\chi}_2^0 \rightarrow \tilde{\ell}_R \ell_1) = 0.63$  (summed over both signs of charge) and  $\text{BR}(\tilde{\ell}_R \rightarrow \tilde{\chi}_1^0 \ell_2) = 1$ . Note that the asymmetry  $\mathcal{A}_T$  and the cross section  $\sigma$  are both considerably enhanced for negative positron and positive electron beam polarization. This choice of polarization enhances the contributions of the right slepton exchange in the neutralino production, Eq. (15), and reduces that of left slepton exchange [40, 41]. While the contributions of right and left slepton exchange enter  $\sigma$  with the same sign, they enter  $\mathcal{A}_T$  with opposite sign, which accounts for the sign change of  $\mathcal{A}_T$ .

In Fig. 11a we show the contour lines of the  $\tau$  polarization asymmetry  $\mathcal{A}_{CP}$ , Eq. (19), for  $\varphi_{A_\tau} = 0.5\pi$  and  $\varphi_{M_1} = \varphi_\mu = 0$  in the  $P_{e^-}$ - $P_{e^+}$  plane. We have chosen a large value of  $|A_\tau| = 1500$  GeV because  $\mathcal{A}_{CP}$  increases with increasing  $|A_\tau| \gg |\mu| \tan\beta$  [36]. For unpolarized beams the asymmetry is 1%. However, it reaches values of more than  $\pm 13\%$  if the  $e^+$  and  $e^-$  beams are polarized with the opposite sign. If at least one of the beams is polarized (e.g.  $P_{e^-} = 0.8$ ,  $P_{e^+} = 0.6$ ), the asymmetries are somewhat smaller ( $\sim 10\%$ ). The reason for

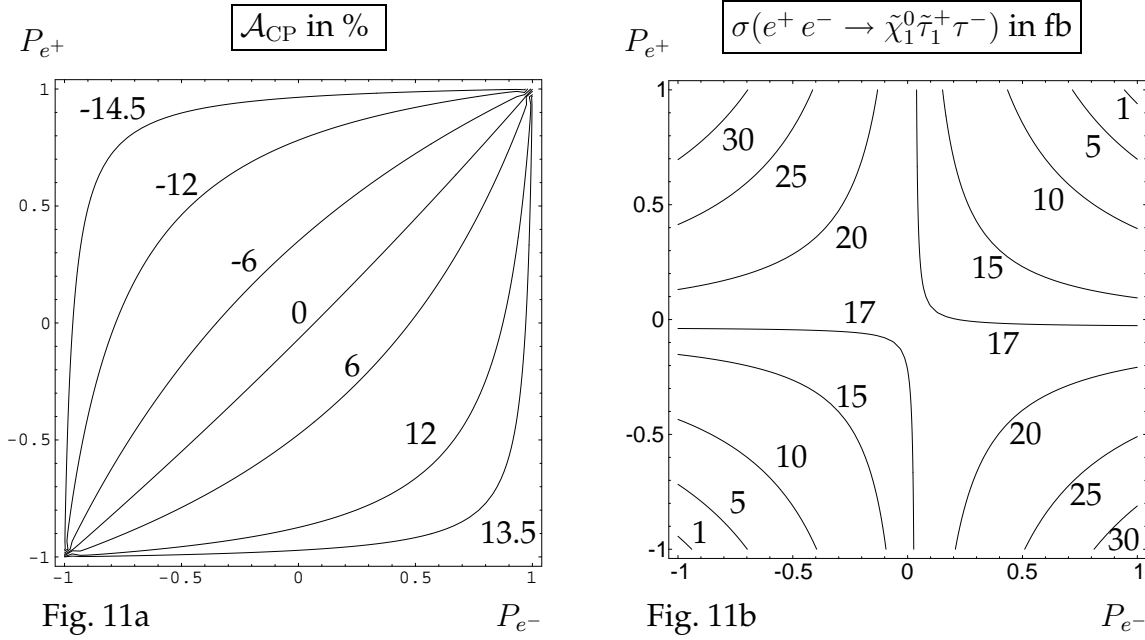


Figure 11: Contour lines of  $\mathcal{A}_{\text{CP}}$  and  $\sigma$  for  $\varphi_{A_\tau} = 0.5\pi$ ,  $|A_\tau| = 1500$  GeV,  $\varphi_{M_1} = \varphi_\mu = 0$ ,  $|\mu| = 250$  GeV,  $M_2 = 200$  GeV,  $\tan\beta = 5$  and  $m_0 = 100$  GeV.

this dependence is again the enhancement of either the right or the left selectron exchange contributions in the production process. The cross section  $\sigma = \sigma(e^+e^- \rightarrow \tilde{\chi}_1^0 \tilde{\chi}_2^0) \times \text{BR}(\tilde{\chi}_2^0 \rightarrow \tilde{\tau}_1^+ \tau^-)$  is shown in Fig. 11b with  $\text{BR}(\tilde{\chi}_2^0 \rightarrow \tilde{\tau}_1^+ \tau^-) = 0.22$ . Also  $\sigma$  is very sensitive to variations of the beam polarization and varies between 1 fb and 30 fb.

Since the asymmetry  $\mathcal{A}_{\text{CP}}$  is also very sensitive to the phases  $\varphi_{M_1}$  and  $\varphi_\mu$  we show for  $\varphi_{M_1} = 0.2\pi$  and  $\varphi_\mu = \varphi_{A_\tau} = 0$ , the dependence of  $\mathcal{A}_{\text{CP}}$  and  $\sigma = \sigma(e^+e^- \rightarrow \tilde{\chi}_1^0 \tilde{\chi}_2^0) \times \text{BR}(\tilde{\chi}_2^0 \rightarrow \tilde{\tau}_1^+ \tau^-)$  on the beam polarization in Figs. 12a, b, respectively. The neutralino branching ratio is  $\text{BR}(\tilde{\chi}_2^0 \rightarrow \tilde{\tau}_1^+ \tau^-) = 0.19$  for our scenario. Despite the small phases,  $\mathcal{A}_{\text{CP}}$  reaches values up to  $-12\%$  for negative  $e^-$  and positive  $e^+$  beam polarizations.

## Summary and conclusion

Within the MSSM we have analyzed the dependence on the beam polarization of two CP-odd asymmetries in  $e^+e^- \rightarrow \tilde{\chi}_1^0 \tilde{\chi}_2^0$  and the subsequent leptonic two-body decay of  $\tilde{\chi}_2^0$ . For the decay process  $\tilde{\chi}_2^0 \rightarrow \tilde{\ell}_R \ell_1$ ,  $\tilde{\ell}_R \rightarrow \tilde{\chi}_1^0 \ell_2$  with  $\ell_{1,2} = e, \mu$ , we have found that the asymmetry  $\mathcal{A}_T$  of the triple product  $(\vec{p}_{e^-} \times \vec{p}_{\ell_2}) \cdot \vec{p}_{\ell_1}$ , which is sensitive to  $\varphi_{M_1}$  and  $\varphi_\mu$ , can be twice as large if polarized beams are used, with e.g.  $P_{e^-} = 0.8$  and  $P_{e^+} = -0.6$ . Also for these polarizations the cross section can be enhanced up to a factor of 2. For the neutralino decay,  $\tilde{\chi}_2^0 \rightarrow \tilde{\tau}_1^\mp \tau^\pm$ , we have given numerical examples for the beam polarization dependence of the CP-odd  $\tau$  polarization asymmetry  $\mathcal{A}_{\text{CP}}$ , which is also sensitive to  $\varphi_{A_\tau}$ . For the scenarios considered, both  $\mathcal{A}_{\text{CP}}$  and the cross section depend sensitively on the beam polarizations and can be enhanced by a factor between 2 and 3. The dependence on the beam polarizations of the asymmetries  $\mathcal{A}_T$ ,  $\mathcal{A}_{\text{CP}}$  and of the cross sections is due to the contributions from right and left selectron exchange in the neutralino production process. Generally, negative (positive)  $e^-$  and positive (negative)  $e^+$  beam polarization enhances right (left) selectron exchange. Due to the fact that both asymmetries and cross

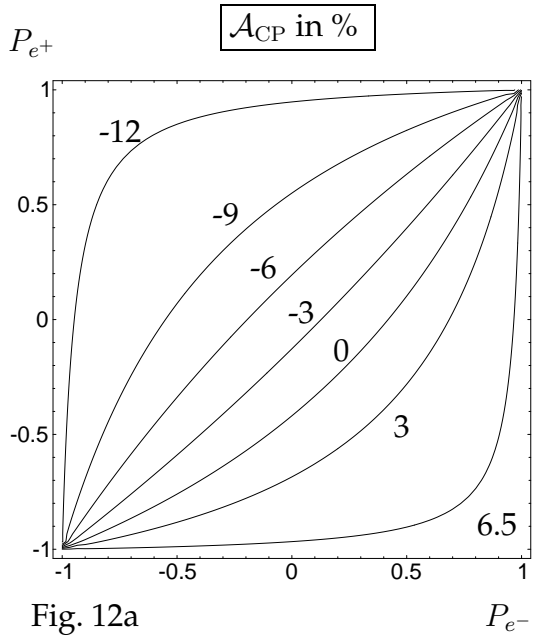


Fig. 12a

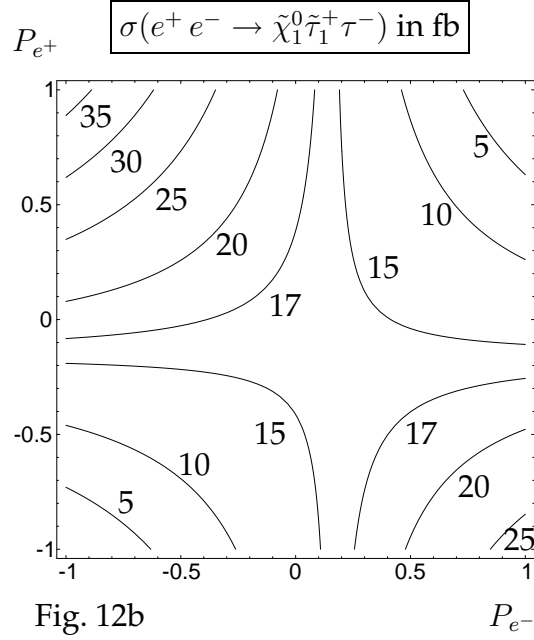


Fig. 12b

Figure 12: Contour lines of  $\mathcal{A}_{\text{CP}}$  and  $\sigma$  for  $\varphi_{M_1} = 0.2\pi$ ,  $\varphi_\mu = 0$ ,  $|\mu| = 250$  GeV,  $M_2 = 200$  GeV,  $\varphi_{A_\tau} = 0$ ,  $|A_\tau| = 250$  GeV,  $\tan\beta = 5$  and  $m_0 = 100$  GeV.

sections can be enhanced significantly, we conclude that the option of having both beams polarized at an  $e^+e^-$ -collider is advantageous for the determination of the CP-odd asymmetries.

## 2.7 CP asymmetries in Neutralino Production and 3-body Decay

Complex parameters in the Minimal Supersymmetric Standard Model (MSSM) introduce new CP-violating effects [30]. CP-odd observables defined with the help of triple products of momenta of the involved particles offer a possibility to study these CP-violating effects [42,43]. In this note we focus on the effects of a complex  $U(1)$  gaugino mass parameter  $M_1$  and higgsino mass parameter  $\mu$  in neutralino production and decay. We analyse the production process

$$e^+ + e^- \longrightarrow \tilde{\chi}_1^0 + \tilde{\chi}_2^0 \quad (20)$$

and subsequent leptonic three-body decay

$$\tilde{\chi}_2^0 \longrightarrow \tilde{\chi}_1^0 + l^- + l^+, \quad (21)$$

where  $l = e, \mu$ . The amplitude squared of the combined processes of production and decay can be written as

$$|T|^2 = PD + \Sigma_P^a \Sigma_D^a, \quad (22)$$

where  $P$  and  $D$  describe production and decay without spin correlation and  $\Sigma_P^a$  and  $\Sigma_D^a$  ( $a = 1, 2, 3$ ) are the terms with spin correlation [44]. In  $\Sigma_P^a$  and  $\Sigma_D^a$  products like  $i\epsilon_{\mu\nu\rho\sigma} p_i^\mu p_j^\nu p_k^\rho p_l^\sigma$  appear. This leads to CP-violating effects already at tree level. We introduce the triple product  $\vec{p}_{l^+}(\vec{p}_{e^-} \times \vec{p}_{l^-})$ , where  $\vec{p}_{e^-}$ ,  $\vec{p}_{l^-}$  and  $\vec{p}_{l^+}$  are the momenta of initial  $e^-$  beam and the two final leptons  $l^-$  and  $l^+$ , respectively. We define a CP asymmetry as

$$A_T = \frac{\int \text{sign}\{\vec{p}_{l^+}(\vec{p}_{e^-} \times \vec{p}_{l^-})\} |T|^2 d\text{lips}}{\int |T|^2 d\text{lips}}, \quad (23)$$

assuming that final state interactions and finite-widths effects can be neglected.  $A_T$  is proportional to the difference of the number of events with the final lepton  $l^+$  above and below the plane spanned by  $\vec{p}_{e^-}$  and  $\vec{p}_{l^-}$ . The analogous asymmetry for neutralino two-body decays has been studied in [45].

### Numerical Results

We analyse the influence of longitudinal beam polarization on the CP asymmetry  $A_T$  in the scenarios defined in Tab.1. Scenario A is inspired by the SPS1a scenario [28], whereas in scenario B the mixing between gaugino and higgsino components is larger. We fix the center of mass energy  $\sqrt{s} = 500$  GeV and take the phases of the complex parameters  $M_1 = |M_1|e^{i\phi_{M_1}}$  and  $\mu = |\mu|e^{i\phi_\mu}$  as  $\phi_{M_1} = \frac{\pi}{2}$  and  $\phi_\mu = 0$ . In Fig.1a and b we show the CP asymmetry  $A_T$ , eq.(4), as a function of the  $e^-$  beam polarization  $P_{e^-}$  for different  $e^+$  beam polarizations  $P_{e^+}$ , in the ranges  $-0.9 \leq P_{e^-} \leq +0.9$  and  $-0.6 \leq P_{e^+} \leq +0.6$ , for the scenarios A and B. In both scenarios the highest CP asymmetry is reached for  $P_{e^-} = -0.9$  and  $P_{e^+} = +0.6$ . For these polarizations the  $\tilde{e}_L$  contributions to the spin density matrix dominate. With opposite signs of the beam polarizations the  $\tilde{e}_R$  contributions are dominating. For scenario A (Fig.1a) one gets a CP asymmetry of about 14%(-2%) for the polarizations  $P_{e^-} = -0.9(+0.9)$  and  $P_{e^+} = +0.6(-0.6)$ . In scenario B (Fig.1b) the CP asymmetry is about 3% in the unpolarized case whereas it is 5%(-3%) with polarizations  $P_{e^-} = -0.9(+0.9)$  and  $P_{e^+} = +0.6(-0.6)$ . Fig.1c and d show the corresponding production cross sections

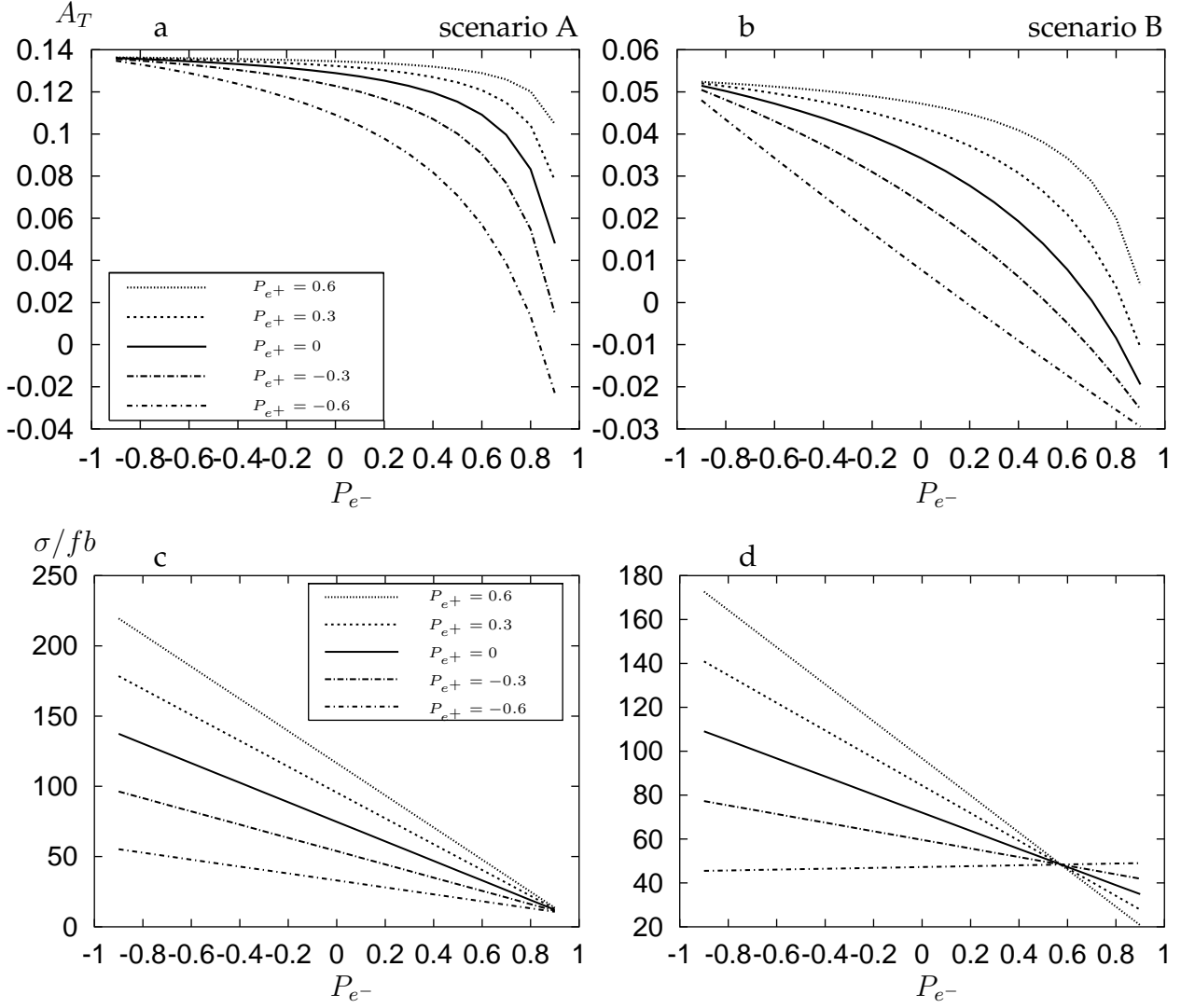


Figure 13: a,b CP asymmetry  $A_T$ , eq.(4), for  $e^+e^- \rightarrow \tilde{\chi}_1^0\tilde{\chi}_2^0$  with subsequent leptonic three-body decay  $\tilde{\chi}_2^0 \rightarrow \tilde{\chi}_1^0 l^+ l^-$ , and c,d production cross section  $\sigma(e^+e^- \rightarrow \tilde{\chi}_1^0\tilde{\chi}_2^0)$ , as a function of the  $e^-$  beam polarization  $P_{e^-}$  for different  $e^+$  beam polarizations  $P_{e^+}$ , for  $\sqrt{s} = 500$  GeV,  $\phi_{M_1} = \frac{\pi}{2}$  and  $\phi_\mu = 0$  for the scenarios A and B defined in Tab.1.

$\sigma$  as a function of the beam polarizations for the same parameters as in Fig.1a and b. In scenario A(B) the cross section and hence the expected rate necessary to measure  $A_T$  is enhanced by  $e^-$  beam polarization  $P_{e^-} = -0.9$  by a factor 1.8(1.6) compared to the unpolarized case. In addition, a polarized  $e^+$  beam with  $P_{e^+} = +0.6$  would further enhance the cross section by a factor 1.5(1.6).

## Summary and Conclusion

We have analysed the dependence on longitudinal beam polarizations of the CP asymmetry  $A_T$ , eq.(4), in neutralino production with subsequent leptonic three-body decay. Our framework has been the MSSM with complex parameters  $M_1$  and  $\mu$ . By changing the beam polarizations it is possible to increase the  $\tilde{e}_L$  or  $\tilde{e}_R$  contributions. We obtain the highest cross section and CP asymmetry with beam polarizations  $P_{e^-} = -0.9$  and

$P_{e^+} = +0.6$ . Then in scenario A(B) the CP asymmetry is enhanced by a factor 1.1(1.5) and the cross section is enhanced by a factor 2.9(2.4) compared to the unpolarized case.

## **Acknowledgements**

We are grateful to H. Fraas, T. Kernreiter, O. Kittel, W. Majerotto and G. Moortgat-Pick for valuable discussions. This work is supported by the 'Fonds zur Förderung der wissenschaftlichen Forschung' (FWF) of Austria, projects No. P13139-PHY and No. P16592-N02 and by the European Community's Human Potential Programme under contract HPRN-CT-2000-00149.

	$ M_1 $	$M_2$	$ \mu $	$\tan \beta$	$m_{\tilde{e}_L}$	$m_{\tilde{e}_R}$	$m_{\tilde{\chi}_1^0}$	$m_{\tilde{\chi}_2^0}$
A	99.1	192.7	352.4	10	267.6	224.4	97.4	176.3
B	100.1	210	250	5	277.4	227.7	96	166.7

Table 2.1: Parameters  $|M_1|$ ,  $M_2$ ,  $|\mu|$ ,  $\tan \beta$ ,  $m_{\tilde{e}_L}$  and  $m_{\tilde{e}_R}$  in the scenarios A and B and the corresponding masses of  $m_{\tilde{\chi}_{1,2}^0}$ . All masses are given in [GeV].

## 2.8 Production of Singlino-dominated Neutralinos with Polarized Beams

Nonminimal extensions of the Minimal Supersymmetric Standard Model (MSSM) are characterized by an additional singlet superfield with vacuum expectation value  $x$ . The singlino character of these singlino-dominated neutralinos crucially depend on the parameter  $x$ . In the Next-to-Minimal Supersymmetric Standard Model (NMSSM) [18–21] or an  $E_6$  inspired model with one extra neutral gauge boson  $Z'$  and one additional singlet superfield [22] neutralinos with a dominant singlet higgsino (singlino) component exist for large values  $x \gtrsim 1$  TeV. Since the singlino component does not couple to gauge bosons, gauginos, (scalar) leptons and (scalar) quarks, cross sections for the production of the exotic neutralinos are generally small [23–26]. However, they may be produced at a high luminosity  $e^+e^-$  linear collider with cross sections sufficient for detection, which can even be enhanced by the use of one or both beams polarized. We analyze the regions of  $x$  where the associated production of the singlino-dominated neutralino yields detectable cross sections for different beam polarisations in scenarios where the MSSM-like neutralinos have similar masses and mixing character as in the ‘typical mSUGRA’ SPS 1a scenario for the MSSM [27, 28].

### Production of singlino-dominated neutralinos

In the NMSSM the parameters (for details see [18])  $M_1 = 99$  GeV,  $M_2 = 193$  GeV,  $\tan \beta = 10$ , the effective  $\mu$  parameter  $\mu_{\text{eff}} = \lambda x = 352$  GeV and the selectron masses  $m_{\tilde{e}_R} = 143$  GeV and  $m_{\tilde{e}_L} = 202$  GeV are chosen according to the scenario SPS 1a. For large  $x \gg |M_2|$  a singlino-dominated neutralino  $\tilde{\chi}_S^0$  with mass  $\approx 2\kappa x$  in zeroth approximation decouples in the neutralino mixing matrix while the other four neutralinos  $\tilde{\chi}_{1,\dots,4}^0$  have MSSM character as in SPS 1a with masses 96 GeV, 177 GeV, 359 GeV and 378 GeV.

Further we consider an  $E_6$  inspired model with one extra neutral gauge boson  $Z'$  and one additional singlet superfield which contains six neutralinos [22]. Again the MSSM parameters and masses of the MSSM-like neutralinos are fixed according to the scenario SPS 1a, while a nearly pure light singlino-like neutralino  $\tilde{\chi}_S^0$  with mass  $\approx 0.18 x^2/|M'|$  in zeroth approximation exists for very large values  $|M'| \gg x$  [29]. The sign of  $M'$  is fixed by requiring relative sign +1 between the mass eigenvalues of  $\tilde{\chi}_S^0$  and  $\tilde{\chi}_1^0$  [23].

In Fig. 14 we show the associated production of the singlino-dominated  $\tilde{\chi}_S^0$  together with the lightest MSSM-like neutralino  $\tilde{\chi}_1^0$  for unpolarized beams and beam polarizations  $P_- = +0.8, P_+ = 0$  and  $P_- = +0.8, P_+ = -0.6$  for two masses 70 and 120 GeV of  $\tilde{\chi}_S^0$ , where the singlino-dominated neutralino is the LSP and NLSP, respectively. Electron beam polarisation  $P_- = +0.8$  enhances the cross section by a factor 1.5 to 1.8, while additional positron beam polarisation  $P_+ = -0.6$  gives a further enhancement factor of about 1.6. The cross sections are decreasing in good approximation as  $1/x^2$  governed by the gaugino content of  $\tilde{\chi}_S^0$  [23, 24]. If we assume a cross section of 1 fb to be sufficient for discovery, the singlino-dominated neutralino can be detected with unpolarized beams for  $x < 7.4$  TeV (9.7 TeV) in the NMSSM with  $m_{\tilde{\chi}_S^0} = 70$  GeV (120 GeV) and for  $x < 8.5$  TeV (6.4 TeV) in the  $E_6$  model. For polarized electron beam the reach in  $x$  is enhanced to  $x < 10.0$  TeV (12.3 TeV) in the NMSSM and  $x < 11.4$  TeV (7.9 TeV) in the  $E_6$  model, whereas for both beams polarized to  $x < 12.6$  TeV (15.5 TeV) in the NMSSM and  $x < 14.4$  TeV (10.0 TeV)

in the  $E_6$  model. Direct experimental evidence of a fifth neutralino would be an explicit proof for an extended SUSY model and is also crucial to apply sum rules in order to test the closure of the neutralino system [30].

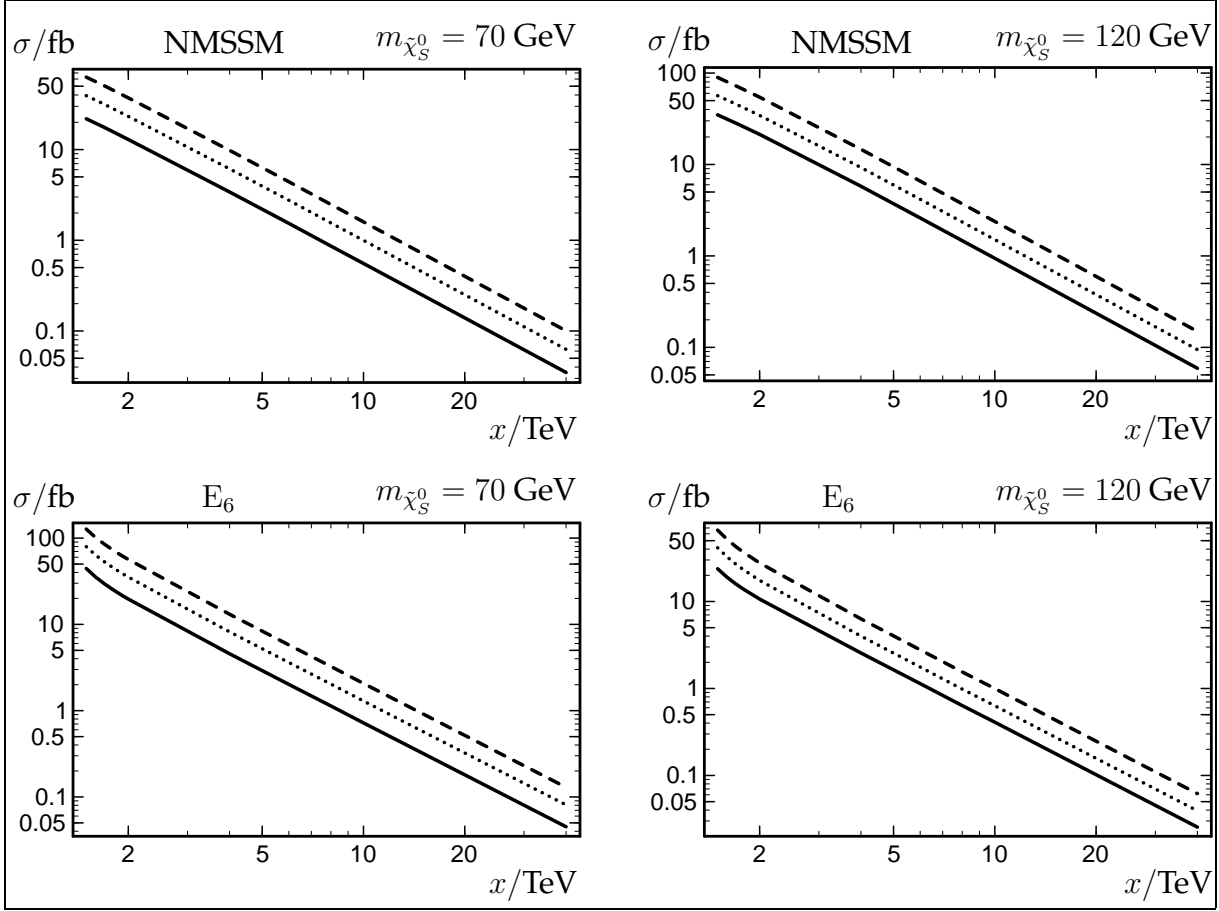


Figure 14: Cross sections for the production of a singlino-dominated neutralino  $\tilde{\chi}_S^0$  via  $e^+e^- \rightarrow \tilde{\chi}_S^0\tilde{\chi}_1^0$  for  $\sqrt{s} = 500$  GeV in the SPS 1a inspired scenarios in the NMSSM and  $E_6$  model with  $M_1 = 99$  GeV,  $M_2 = 193$  GeV,  $\tan\beta = 10$  and  $\mu_{\text{eff}} = \lambda x = 352$  GeV with unpolarized beams (solid) and beam polarizations  $P_- = +0.8, P_+ = 0$  (dotted) and  $P_- = +0.8, P_+ = -0.6$  (dashed). The mass of  $\tilde{\chi}_S^0$  is fixed at 70 GeV and 120 GeV by the parameters  $\kappa$  (NMSSM) and  $M'$  ( $E_6$  model).

## Conclusion

We have studied the production of singlino-dominated neutralinos in the NMSSM and an  $E_6$  inspired model at a linear collider with polarized beams. With both beams polarized the cross sections are enhanced by a factor 2.4 – 2.9 in comparison to unpolarized beams, depending on the scenario. This enhances the reach for the singlino-dominated neutralinos to singlet vevs as large as 15 TeV.

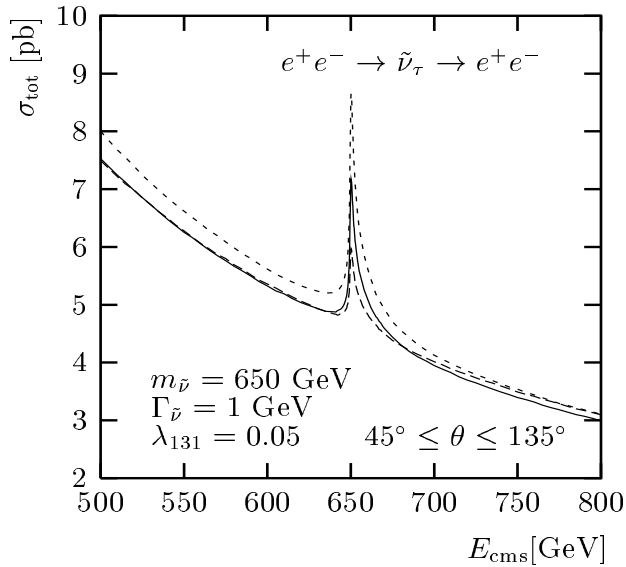


Figure 15: SUSY – Sneutrino production in R–parity violating model: Resonance production of  $e^+e^- \rightarrow \tilde{\nu}$  interfering with Bhabha scattering for different configurations of beam polarization: unpolarized case (solid),  $P_{e^-} = -80\%$  and  $P_{e^+} = +60\%$  (hatched),  $P_{e^-} = -80\%$  and  $P_{e^+} = -60\%$  (dotted) [31].

## 2.9 Polarization effects in R–parity violating SUSY

In R–parity violating SUSY, processes can occur which prefer the extraordinary (LL) or (RR) polarization configurations. An interesting example is  $e^+e^- \rightarrow \tilde{\nu} \rightarrow e^+e^-$ . The main background to this process is Bhabha scattering. Polarizing both electrons and positrons can strongly enhance the signal. A study [31] was made for  $m_{\tilde{\nu}} = 650$  GeV,  $\Gamma_{\tilde{\nu}} = 1$  GeV, with an angle cut of  $45^\circ \leq \Theta \leq 135^\circ$  and a lepton–number violating coupling  $\lambda_{131} = 0.05$  in the R–parity violating Lagrangian  $\mathcal{L}_R \sim \sum_{i,j,k} \lambda_{ijk} L_i L_j E_k$ . Here  $L_{i,j}$  denotes the left–handed lepton and squark superfield and  $E_k$  the corresponding right–handed field [31]. The resonance curve for the process, including the complete SM–background is given in Figure 15. The event rates at the peak are given in Table 2.2. Electron polarization with  $(-80, 0)$  enhances the signal only slightly by about 2%, whereas the simultaneous polarization of both beams with  $(-80, -60)$  produces a further increase by about 20%. The background changes only slightly due to the t–channel (LL) contributions from  $\gamma$  and  $Z$  exchange.

This configuration of beam polarizations, which strongly suppresses pure SM processes, allows one to perform fast diagnostics for this R–parity violating process. For example the process  $e^+e^- \rightarrow Z'$  could lead to a similar resonance peak, but with different polarization dependence. Here only the ‘normal’ configurations  $LR$  and  $RL$  play a role and this process will be strongly suppressed by  $LL$ . Therefore such a resonance curve, Figure 15, with different beam polarizations would uniquely identify an R–parity violating SUSY process.

Table 2.2: SUSY – Sneutrino production in R-parity violating SUSY: Cross sections of  $e^+e^- \rightarrow \tilde{\nu} \rightarrow e^+e^-$  for unpolarized beams,  $P_{e^-} = -80\%$  and unpolarized positrons and  $P_{e^-} = -80\%, P_{e^+} = -60\%$ . The study was made for  $m_{\tilde{\nu}} = 650$  GeV,  $\Gamma_{\tilde{\nu}} = 1$  GeV, an angle cut of  $45^\circ \leq \theta \leq 135^\circ$  and the R-parity violating coupling  $\lambda_{131} = 0.05$  [31].

	$\sigma(e^+e^- \rightarrow e^+e^-)$ with $\sigma(e^+e^- \rightarrow \tilde{\nu} \rightarrow e^+e^-)$	Bhabha-background
unpolarized	7.17 pb	4.50 pb
$P_{e^-} = -80\%$	7.32 pb	4.63 pb
$P_{e^-} = -80\%, P_{e^+} = -60\%$	8.66 pb	4.69 pb
$P_{e^-} = -80\%, P_{e^+} = +60\%$	5.97 pb	4.58 pb

## 2.10 Production of heavy Higgs bosons in weak boson fusion

The possibility to enhance cross sections by using beam polarization can be very important for detecting processes with a very low rate. In Ref. [17] the production of the heavy neutral  $\mathcal{CP}$ -even Higgs boson  $H$  of the MSSM was studied. Since for large values of the  $\mathcal{CP}$ -odd Higgs boson mass  $M_A$  the heavy Higgs bosons  $A$  and  $H$  are approximately mass degenerate,  $M_A \approx M_H$ , the pair production channel  $e^+e^- \rightarrow HA$  is limited by kinematics to the region  $M_H < \sqrt{s}/2$ . The kinematic limit of the LC can in principle be extended by single Higgs production in the process  $e^+e^- \rightarrow \nu\bar{\nu}H$ . However, due to the decoupling properties of the heavy Higgs bosons for  $M_A \gg M_Z$  the  $VVH$  coupling ( $V = W^\pm, Z$ ) is very small, so that the process  $e^+e^- \rightarrow \nu\bar{\nu}H$  has only a very low rate.

In Ref. [17] it was shown that higher-order contributions to this Higgs-boson production process can remedy this situation, making the process potentially accessible at the LC. This requires a high integrated luminosity and polarized beams. The cross section becomes enhanced for left-handedly polarized electrons and right-handedly polarized positrons. While an 80% polarization of the electron beam alone results in a cross section that is enhanced by a factor 1.8, the polarization of both beams, i.e. 80% polarization for electrons and 60% polarization for positrons, would yield roughly an enhancement by a factor of 2.9. With an anticipated integrated luminosity of the LC running at its highest energy of  $\mathcal{O}(2\text{ab}^{-1})$  the enhancement in the cross section due to the beam polarization can extend the kinematic reach of the LC by roughly 100 GeV compared to the case of unpolarized beams.

Table 2.3:  $1\sigma$  statistical errors in units of  $10^{-3}$  on the real parts of  $CP$  conserving TGCs in the presence of all anomalous couplings at  $\sqrt{s} = 500$  GeV, with unpolarised beams and with different beam polarisations.

	Re $\Delta g_1^\gamma$	Re $\Delta g_1^Z$	Re $\Delta \kappa_\gamma$	Re $\Delta \kappa_Z$	Re $\lambda_\gamma$	Re $\lambda_Z$	Re $g_5^\gamma$	Re $g_5^Z$
no polarisation	6.5	5.2	1.3	1.4	2.3	1.8	4.4	3.3
$(P_l^-, P_l^+) = (\mp 80\%, 0)$	3.2	2.6	0.61	0.58	1.1	0.86	2.2	1.7
$(P_l^-, P_l^+) = (\mp 80\%, \pm 60\%)$	1.9	1.6	0.40	0.36	0.62	0.50	1.4	1.1
$(P_t^-, P_t^+) = (80\%, 60\%)$	2.8	2.4	0.69	0.82	0.69	0.55	2.5	1.9

## 2.11 Triple gauge boson couplings

An important feature of the electroweak Standard Model (SM) is the non-Abelian nature of its gauge group, which gives rise to gauge boson self-interactions, in particular to the triple gauge couplings (TGCs)  $\gamma WW$  and  $ZWW$ . The most general vertices contain altogether 14 complex parameters [71], six of them  $CP$  violating. The SM predicts only four  $CP$  conserving real couplings to be non-zero at tree level. A precision measurement of the TGCs at high energies will be a crucial test of the validity of the SM, given that a variety of new physics effects can manifest itself by deviations from the SM predictions (for references see e.g. [72]). Though no deviation from the SM has been found for the TGCs from LEP data [73], the bounds obtained are comparatively weak. The tightest bounds on the anomalous couplings, i.e. on the differences between a coupling and its SM value, are of order 0.05 for  $\Delta g_1^Z$  and  $\lambda_\gamma$ , of order 0.1 for  $\Delta \kappa_\gamma$  and of order 0.1 to 0.6 for the real and imaginary parts of  $C$  and/or  $P$  violating couplings. These numbers correspond to fits where all anomalous couplings except one are set to zero. Moreover, many couplings, e.g. the imaginary parts of  $C$  and  $P$  conserving couplings, have been excluded from the analyses so far.

At a future linear  $e^+e^-$  collider one will be able to study these couplings with unprecedented accuracy. A process particularly suitable for this is  $W$  pair production where both the  $\gamma WW$  and the  $ZWW$  couplings can be measured at the scale given by the c.m. energy  $\sqrt{s}$ . In two recent papers the prospects to measure the full set of 28 (real) TGCs in this reaction is systematically investigated for unpolarised beams as well as for longitudinal [72] and transverse [74] beam polarisation. In these two studies optimal observables are used, which are constructed to give the smallest possible statistical errors for a given event distribution [75]. In addition, they take advantage of the discrete symmetries of the differential cross section. In  $W$  pair production the covariance matrix of these observables consists of four blocks that correspond to  $CP$  even or  $CP$  odd TGCs and to their real or imaginary parts. Within each block all correlations between couplings are taken into account.

Table 2.3 shows the errors on the real parts of  $CP$  conserving TGCs at  $\sqrt{s} = 500$  GeV with unpolarised beams and with different beam polarisations, assuming an integrated luminosity of  $500 \text{ fb}^{-1}$ . Here, only those events are considered where one  $W$  boson decays into a quark-antiquark pair and the other one into  $e\nu$  and  $\mu\nu$ . It is further assumed that the two jets of the hadronic  $W$  decay cannot be identified as originating from the up- and down-type (anti)quark. In the case of longitudinal polarisation the luminosity is distributed equally on both directions of the polarisation vectors and the results are then combined.

Table 2.4: Same as Table 2.3, but for the imaginary parts and with the L-R-parameterisation.

	$\text{Im } g_1^L$	$\text{Im } \kappa_L$	$\text{Im } \lambda_L$	$\text{Im } g_5^L$	$\tilde{h}_-$	$\tilde{h}_+$	$\text{Im } \lambda_R$	$\text{Im } g_5^R$
no polarisation	2.7	1.7	0.48	2.5	11	—	3.1	17
$(P_l^-, P_l^+) = (\mp 80\%, 0)$	2.6	1.2	0.45	2.0	4.5	—	1.4	4.3
$(P_l^-, P_l^+) = (\mp 80\%, \pm 60\%)$	2.1	0.95	0.37	1.6	2.5	—	0.75	2.3
$(P_t^-, P_t^+) = (80\%, 60\%)$	2.6	1.2	0.46	2.0	3.7	3.2	0.98	4.4

The errors with unpolarised beams are between  $10^{-3}$  and  $10^{-2}$  in the parameterisation using photon and  $Z$  couplings. At 800 GeV all errors (with or without polarisation) are smaller, notably for  $\text{Re } \Delta\kappa_\gamma$ . For both c.m. energies the errors on the couplings in the  $\gamma$ - $Z$ -parameterisation decrease by about a factor 2 when going from unpolarised beams to longitudinal  $e^-$  polarisation and an unpolarised  $e^+$  beam. Going from unpolarised beams to polarised  $e^-$  and  $e^+$  this factor is between 3 and 4 for all couplings, except for  $\text{Re } \Delta\kappa_Z$  at 800 GeV where it is 4.7. If both beams have transverse polarisation, the errors on most couplings are approximately of the same size as in the situation where only the  $e^-$  beam has longitudinal polarisation. Only for  $\text{Re } \lambda_\gamma$ ,  $\text{Re } \lambda_Z$ ,  $\text{Re } \tilde{\lambda}_\gamma$  and  $\text{Re } \tilde{\lambda}_Z$  are they smaller, viz. they are of the same size as with both beams longitudinally polarised. This is true for both energies. If electron as well as positron polarisation is available we thus conclude that, regarding the  $1\sigma$ -standard deviations on the TGCs (without assuming any coupling to be zero) *longitudinal* polarisation is the preferable choice, apart from one exception (see below). Note that we are better with longitudinal polarisation also for all  $CP$  violating couplings.

It has been emphasized [75] that the following linear combinations [71] can be measured with much smaller correlations than the  $\gamma$ - $Z$  couplings:

$$\begin{aligned} g_1^L &= 4 \sin^2 \theta_W g_1^\gamma + (2 - 4 \sin^2 \theta_W) \xi g_1^Z, \\ g_1^R &= 4 \sin^2 \theta_W g_1^\gamma - 4 \sin^2 \theta_W \xi g_1^Z, \end{aligned} \quad (24)$$

where  $\xi = s/(s - m_Z^2)$ , and similarly for the other couplings. The L- and R-couplings respectively appear in the amplitudes for left- and right-handed initial  $e^-$ . Therefore this parameterisation seems to be more “natural” in the presence of beam polarisation than the conventional one. For detailed plots showing the sensitivity to the TGCs as a function of the degree of longitudinal polarisation we refer to [72]. There an extended optimal-observable method [76] has been used where correlations between TGCs are eliminated through appropriate energy- and polarisation-dependent reparameterisations.

For the imaginary parts of the  $CP$  conserving couplings, see Table 2.4, we further use the linear combinations  $\tilde{h}_\pm = \text{Im}(g_1^R \pm \kappa_R)/\sqrt{2}$  instead of  $\text{Im } g_1^R$  and  $\text{Im } \kappa_R$ . It has been shown in [72] that  $\tilde{h}_+$  is not measurable from the normalised event distribution, neither with unpolarised beams nor with longitudinal polarisation. One can however measure this coupling with *transverse* beam polarisation with good sensitivity. In the  $\gamma$ - $Z$ -parameterisation this means that the four couplings  $\text{Im } g_1^\gamma$ ,  $\text{Im } g_1^Z$ ,  $\text{Im } \kappa_\gamma$  and  $\text{Im } \kappa_Z$  are not simultaneously measurable without transverse polarisation.

Although for most couplings longitudinal polarisation of both beams is the advantageous choice, measurement of the full parameter space requires to spend part of the total luminosity of the collider on the transverse polarisation mode.

For comparison with a simulation of determining the charged current triple gauge couplings via a fit see also [77].

## 2.12 Probing New Physics with Transverse Polarization via CP violation (plots+some more text are coming)

This is a précis of a recent preprint [70]. Transverse polarization (TP) enables novel CP violation search in the inclusive process  $e^+e^- \rightarrow A + X$ . When the spin of  $A$  is unobserved and  $m_e$  is neglected, only (pseudo-)scalar or tensor currents associated with a new-physics scale  $\Lambda$  can lead to CP-odd observables at leading order in the couplings from interference with  $\gamma$  and  $Z$  in the presence of TP. In order to test CP violation, one needs more than the momenta of particles to be measured in  $e^+e^- \rightarrow f\bar{f}$ . The presence of TP provides such a vector, without observing final state polarization. This leads to gain in statistics. CP violation due to beyond the standard model interactions may be parametrized in terms of contact interactions in a model independent manner. When  $m_e$  is neglected, with only TP interactions that transform as V and A cannot interfere at leading order in the new interactions with the standard model interactions to yield CP odd correlations, which can be inferred from general results of Dass and Ross. We have evaluate the contributions to the differential cross-section due to (pseudo)-scalar and tensor contact interactions at leading order in the interaction strengths for the process  $e^+e^- \rightarrow t\bar{t}$ . This is used to construct an effective up-down asymmetry and a polar angle integrated version of the same. By assuming that the coefficients of the effective interaction that is suppressed by the second power of the new-physics scale  $\Lambda$ , to be of order unity, we show that at  $\sqrt{s} = 500$  GeV and with an integrated luminosity  $\int dt\mathcal{L} = 500 \text{ fb}^{-1}$ , we find that at the 90% confidence level, the scale  $\Lambda$  can be bounded at about 10 TeV, with perfect TP.

## 2.13 Transverse Polarization and Extra Dimensions at Linear Colliders

New Physics beyond the Standard Model (SM) is expected to lie at or near the TeV scale. Once this scale is probed by future colliders, such as the LHC and the Linear Collider (LC), this new physics should begin to show itself. What is uncertain is the form this manifestation will take. The most straightforward scenario would be the production of new particles such as SUSY or Kaluza-Klein resonances. A second possibility is that new processes which are not allowed within the SM framework will begin to be observed. Lastly, one can imagine that the data begins show small deviations from the SM predictions for various observables, *e.g.*, cross sections and asymmetries, which grow with increasing energy. This last possibility signals the existence of new physics beyond the kinematic reach of the collider which is manifesting itself in the form of higher dimensional operators, *i.e.*, contact interactions. These operators can arise from the exchanges of new particles, with different spins and in various channels depending upon the particular model. From the literature it is easy to construct a rather long list of potential new physics scenarios of this type: a  $Z'$  from an extended gauge model [78,79], scalar or vector leptoquarks [78,80],  $R$ -parity violating sneutrino( $\tilde{\nu}$ ) exchange [81], scalar or vector bileptons [82], graviton Kaluza-Klein(KK) towers [83,84] in extra dimensional models [85,86], gauge boson KK towers [84,87], and even string excitations [88].

If such deviations are observed it will be necessary to have techniques available to differentiate the multiple possibilities experimentally and point us in the direction of the correct scenario. One possible path to take is to compare the observed shifts with the predictions of all of the currently available models [89]. An alternative to this approach is to develop specific tools to rapidly identify certain classes of models which lead to uniquely distinct signatures. In this paper we examine one such tool which becomes available at the LC provided both the  $e^-$  and  $e^+$  beams are initially longitudinally polarized and spin rotators are used to convert these to transversely polarized beams. As we will see below, transverse polarization (TP) [90] allows for new asymmetries to be constructed which are associated with the azimuthal angle formed by the directions of the  $e^\pm$  polarization and the plane of the momenta of the outgoing fermions in the  $e^+e^- \rightarrow f\bar{f}$  process. Historically, the possible use of TP as a tool for new physics searches and analyses has not gotten the attention it deserves in the literature [90]. Here we are interested in using the associated TP asymmetries to uniquely probe for the  $s$ -channel exchange of spin-2 fields in  $e^+e^-$  collisions which we normally associate with the Kaluza-Klein graviton towers of the Arkani-Hamed, Dimopoulos and Dvali(ADD) [85] or Randall-Sundrum(RS) [86] scenarios.

### Transverse Polarization Asymmetries

For our analysis we will follow a slightly modified version of the notations and conventions employed by Hikasa [90]. Consider the process  $e^+e^- \rightarrow f\bar{f}$  with the both electron and positron beams polarized. We will denote the linear and transverse components of the  $e^-$  ( $e^+$ ) polarizations by  $P_{L,T}$  ( $P'_{L,T}$ ) and for simplicity assume that the two transverse polarization vectors are parallel up to a sign. In this case, the spin-averaged matrix ele-

ment for this process can be written as

$$|\bar{\mathcal{M}}|^2 = \frac{1}{4}(1 - P_L P'_L)(|T_+|^2 + |T_-|^2) + (P_L - P'_L)(|T_+|^2 - |T_-|^2) + (2P_T P'_T)[\cos 2\phi \operatorname{Re}(T_+ T_-^*) - \sin 2\phi \operatorname{Im}(T_+ T_-^*)], \quad (25)$$

where  $\phi$  is the azimuthal angle defined on an event-by-event basis described above. It is interesting to note that the  $\phi$ -dependent pieces of  $|\bar{\mathcal{M}}|^2$  are particularly sensitive to the relative phases between the two sets of amplitudes. We also observe from this expression the important fact that the  $\phi$ -dependent pieces are *only* accessible if both beams are simultaneously transversely polarized. Thus to have azimuthal asymmetries at a LC we must begin with both beams longitudinally polarized and employ spin rotators.

Let us first consider the simple case with massless fermions; we define the quantities

$$\begin{aligned} f_{LL} &= Q_e Q_f + g_Z(v_e - a_e)(v_f - a_f)P \\ f_{RR} &= Q_e Q_f + g_Z(v_e + a_e)(v_f + a_f)P \\ f_{LR} &= Q_e Q_f + g_Z(v_e - a_e)(v_f + a_f)P \\ f_{RL} &= Q_e Q_f + g_Z(v_e + a_e)(v_f - a_f)P, \end{aligned} \quad (26)$$

where  $v_e, a_e(v_f, a_f)$  are the vector and axial vector couplings of the initial electron(final fermion) to the  $Z$  and  $Q_{e,f}$  are their corresponding electric charges, with

$$g_Z = \frac{G_F M_Z^2}{2\sqrt{2}\pi\alpha}, \quad (27)$$

and

$$P = \frac{s}{s - M_Z^2 + iM_Z\Gamma_Z}. \quad (28)$$

Without scalar exchange but allowing for the possibility of spin-2 the relevant helicity amplitudes for this process are given by

$$\begin{aligned} T_{+-}^{+-} &= f_{LL}(1+z) - f_g(z+2z^2-1) \\ T_{+-}^{-+} &= f_{LR}(1-z) - f_g(z-2z^2+1) \\ T_{-+}^{+-} &= f_{RL}(1-z) - f_g(z-2z^2+1) \\ T_{-+}^{-+} &= f_{RR}(1+z) - f_g(z+2z^2-1). \end{aligned} \quad (29)$$

where  $z = \cos\theta$ . Note that the spin-2 exchange merely augments the amplitudes which are already present in the SM(though with different  $\cos\theta$  dependencies), *i.e.*, no new helicity amplitudes are generated by spin-2. In contrast to this, scalar exchange would yield additional amplitudes of the form  $T_{++}^{++}$  *etc.* not present in the SM and would thus be easily isolated using the more conventional asymmetries associated with two beam longitudinal polarization [81].  $f_g$  is a model-dependent quantity; in the usual ADD model, employing the convention of Hewett [83], one finds

$$f_g = \frac{\lambda s^2}{4\pi\alpha M_H^4}. \quad (30)$$

where  $M_H$  represents the cutoff scale in the KK graviton tower sum and  $\lambda = \pm 1$ . In the RS model the corresponding expression can be obtained through the replacement

$$\frac{\lambda}{M_H^4} \rightarrow \frac{-1}{8\Lambda_\pi^2} \sum_n \frac{1}{s - m_n^2 + im_n\Gamma_n}. \quad (31)$$

where  $\Lambda_\pi$  is of order a few TeV and  $m_n(\Gamma_n)$  are the masses(widths) of the TeV scale graviton KK excitations. In what follows we will always assume that we are below the threshold for the production of these resonances otherwise the spin-2 nature of the new exchange would be easily identified through an examination of the resonances themselves. We will also assume that their widths can be neglected in cross section calculations.

In the case of massive final state fermions, such as tops, the helicity amplitudes given above are slightly altered and new amplitudes  $T_{+-}^{\pm\pm}$  and  $T_{-+}^{\pm\pm}$  are also present. They will be included in the analysis in the case of top quark pair production.

What is the form or the angular distribution,  $d\sigma/dz d\phi$ , in the SM? In particular, we are interested in the  $z$ -dependence of the terms associated with  $\cos 2\phi$  and  $\sin 2\phi$  in the expression above when no new physics is present. We note that the a small ‘imaginary’ term will be present even in the SM due to the finite width of  $Z$ . For  $\sqrt{s} \geq 500$  GeV this term can be safely neglected for most of our analyses. As shown in, *e.g.*, the work of Hikasa, both of these  $\phi$ -dependent terms are always proportional to  $1 - z^2$  in the SM and will remain so even if new gauge boson exchanges are present. However, due to the more complex  $z$ -dependence of the spin-2 contributions to the helicity amplitudes we expect significant modifications of the SM result when gravitons are exchanged. In fact, interference between SM and spin-2 exchange amplitudes are found to produce both even and odd- $z$  terms with the latter proportional to  $\sim z(1 - z^2)$  whereas the smaller pure gravity terms are instead found to be even in  $z$  and proportional to  $z^2 - (2z^2 - 1)^2$ . The general difference in the  $z$ -dependence of the of the  $\phi$  sensitive terms and, in particular, the existence of the odd- $z$  contributions is clearly a signal for spin-2 exchange.

Let us assume, as mentioned above, that we are in an energy regime where the effects of the finite width of the  $Z$  can be neglected. For the moment, this would seem to imply that the term proportional to  $\sin 2\phi$  can be neglected in the case of KK graviton exchange. Let us proceed making this assumption but remembering to return to this important point below. We will later see that the terms that we now neglecting will have no influence on this part of our analysis. In order to attempt to isolate the spin-2 exchange contributions we first can form a differential azimuthal asymmetry distribution which we define by

$$\frac{1}{N} \frac{dA}{dz} = \left[ \frac{\int_+ \frac{d\sigma}{dz d\phi} - \int_- \frac{d\sigma}{dz d\phi}}{\int d\sigma} \right], \quad (32)$$

where  $\int_\pm$  are integrations over regions where  $\cos 2\phi$  takes on  $\pm$  values; integration over the full ranges of  $z$  and  $\phi$  occurs in the denominator. It is important to note that we expect this differential asymmetry to take on rather small numerical values since it is normalized to the total cross section and *not* to the differential cross section at the same value of  $z$  as is usually done. As we will see below, this particular normalization is most useful in isolating the most important aspects of TP physics. To get a feeling for this asymmetry, we show its behaviour for both the SM and in the ADD scenario in Fig.1 at a 500 GeV LC for the final states  $f = \mu$  or  $\tau, c$  and  $b$ . Note that from here on we will combine results for the  $f = \mu$  and  $\tau$  final states to get added statistics. In this figure we have for concreteness assumed that the spin rotators are nearly 100% efficient [91] so that  $P_T = 0.8$  and  $P'_T = 0.6$ . Note that the spin-2 effects are large and in particular the fact that the azimuthal asymmetry distribution is no longer symmetric under  $z \rightarrow -z$  as we might expect from the discussion above.

There are two ways to naively access the odd- $z$  terms. First, one can take the differential azimuthal asymmetry defined above, separately integrate it over positive and nega-

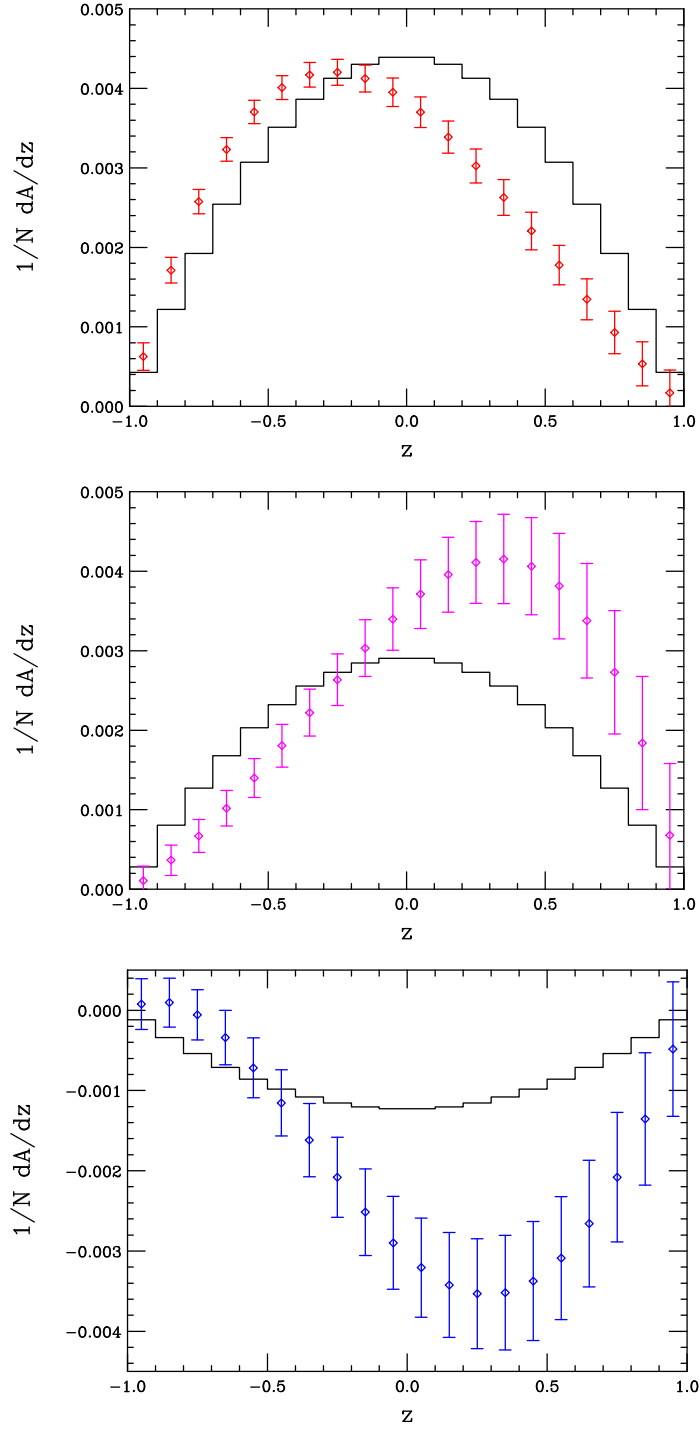


Figure 16: Differential azimuthal asymmetry distribution for  $e^+e^- \rightarrow f\bar{f}$  at a 500 GeV LC assuming a luminosity of  $500 fb^{-1}$ . The histograms are the SM predictions while the data points assume the ADD model with  $M_H = 1.5$  TeV. In the top panel  $f = \mu$  and  $\tau$  are combined, while in the middle(lower) panel,  $f = c(b)$ .  $P_T = 0.8$  and  $P'_T = 0.6$  are assumed.

tive values of  $z$ , then take the difference, *i.e.*, form a forward-backward asymmetry using  $N^{-1}dA/dz$ :

$$A_{FB} = \frac{1}{N} \left[ \int_{z \geq 0} dz \frac{dA}{dz} - \int_{z \leq 0} dz \frac{dA}{dz} \right]. \quad (33)$$

It is important to be reminded that in the SM and in any new physics scenario with  $s$ -channel  $Z'$  exchanges one has  $A_{FB} = 0$ . This is also true in the usual four-fermion contact interaction scenario [93] which involves only vector and axial-vector couplings. Due to the nature of spin-0 exchange it is clear that  $A_{FB}$  would remain zero in this case as well. A second possibility is to take *odd* moments of the asymmetry with respect to, *e.g.*, the Legendre polynomials  $P_n(z)$  [92]:

$$\langle P_n \rangle = \frac{1}{N} \left[ \int dz P_n(z) \frac{dA}{dz} \right]. \quad (34)$$

Note that only  $\langle P_{1,3} \rangle$  will be non-zero in this case since no factors of  $z^5$  appear in the cross section. As in the case of  $A_{FB}$ , these moments are zero in both the SM and  $Z'$  models. In the case of graviton exchange, not only are the moments  $\langle P_{1,3} \rangle$  non-zero, they are also not independent of each other. A short analysis finds that in the case of spin-2 exchange the ratio of moments is fixed:  $\langle P_3 \rangle / \langle P_1 \rangle = -3/7$ , uniquely. It is thus rather obvious that the existence of odd- $z$  terms is a signal for graviton, or more generally, spin-2 exchange.

## Analysis

It is clear that non-zero values of either  $A_{FB}$  or  $\langle P_{1,3} \rangle$  provide a clean signature for spin-2 exchange in the  $e^+e^- \rightarrow f\bar{f}$  process. Their appearance at the level of  $5\sigma$  can thus be claimed as, not just a discovery of new physics, but spin-2 exchange in particular. To be specific in what follows let us concentrate on the ADD model; (almost) all limits obtained there can be immediately translated to the case of the RS scenario. From Fig.1 it is apparent that modest values of  $M_H$  cause quite sizeable distortions in the  $N^{-1}dA/dz$  distribution. However, as we will see this sensitivity is somewhat diluted if we are only asking whether or not, *e.g.*  $A_{FB}$  is non-zero. After all the asymmetry distribution may be quite different than what the SM predicts in both magnitude and shape and yet  $A_{FB}$  will remain zero. Such a possibility will occur in the case of, *e.g.*, spin-0 exchange. To determine the  $5\sigma$  *identification* reach we will assume that the individual polarizations are known rather well,  $\delta P/P = 0.003$ , that the efficiencies of identifying the final state fermions is rather high: 100% for  $f = \mu, \tau$ , 60% for  $f = c, t$ , and 80% for  $f = b$  with no associated systematic uncertainties and include the effects of initial state radiation. The  $5\sigma$  identification reaches, making these assumptions, are shown in Figs. 2 and 3 for different values of  $\sqrt{s}$  as functions of the integrated luminosity. In obtaining these results we have combined all of the various final states above into a single fit. In all cases a small angle cut of 100 mrad around the beam pipe has been employed.

From these two figures some immediate conclusions can be drawn. First, it is clear that the identification reach obtained from  $A_{FB}$  is somewhat superior to that obtained from the measurements of  $\langle P_{1,3} \rangle$ . Secondly, it is clear that the identification reach in either

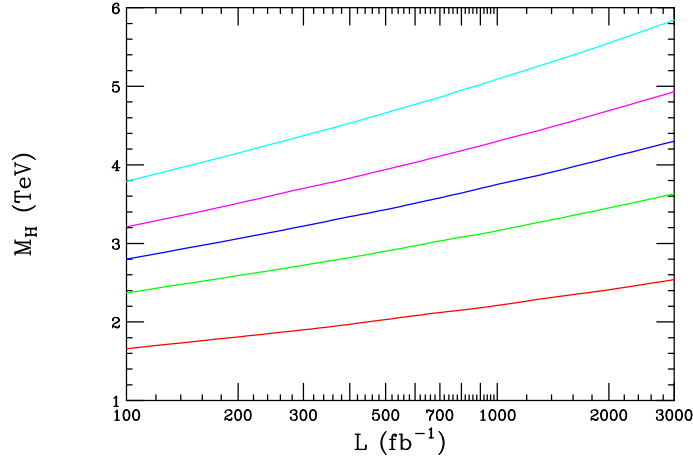


Figure 17:  $5\sigma$  identification reach in  $M_H$  using  $A_{FB}$  as a function of the integrated luminosity from the process  $e^+e^- \rightarrow f\bar{f}$ , with  $f$  summed over  $\mu, \tau, b, c$  and  $t$ . Here  $P_T = 0.8$  and  $P'_T = 0.6$  are assumed. From bottom to top the curves are for  $\sqrt{s} = 0.5, 0.8, 1, 1.2$  and  $1.5$  TeV, respectively.

case alone,  $M_H \sim (3.5 - 4)\sqrt{s}$ , is not as good as what can be obtained employing longitudinal polarization [92]. In order to obtain better reaches we must try something more aggressive.

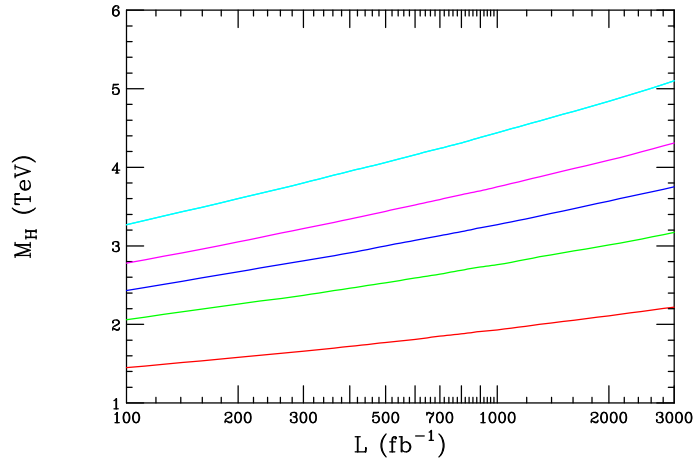


Figure 18: Same as the previous figure but now using the moments  $\langle P_{1,3} \rangle$ .

We noted above that in the SM, in all  $Z'$  models and in the case of conventional four-fermion contact interactions the azimuthal asymmetry always takes the form  $N^{-1}dA/dz \sim (1 - z^2)$ . Clearly these specific forms of new physics will only modify the normalization of the azimuthal asymmetry distribution since its shape is left unaltered. We can thus ask up to what value of the cutoff scale,  $M_H$ , can we differentiate the effects of gravity—a change in the *shape* of these distributions—from a simple overall change in the normalization of distributions for the various final states. This allows us to set a limit on the value of  $M_H$  below which graviton exchange can be distinguished from  $Z'$  exchange or four-fermion contact interactions. To do this we fix  $M_H$  and try to fit the  $N^{-1}dA/dz$  distributions for  $\mu, \tau, c$  and  $b$  final states assuming a SM shape but allowing the normalization to float in-

dependently for each final state. If the CL of the fit is very poor we raise  $M_H$  until we achieve a CL equivalent to  $5\sigma$ , *i.e.*,  $5.7 \times 10^{-5}$ . For luminosities above  $100 - 200 \text{ fb}^{-1}$  the errors are completely dominated by systematics and we find the results shown in Table 1. (Changing the luminosities in our range of interest  $\frac{1}{2} - 2 \text{ fb}^{-1}$  has little quantitative effect and only modifies the second decimal place in these results.) Here we see that for  $M_H \leq (10 - 11)\sqrt{s}$  the effects of spin-2 graviton exchange can be distinguished from a  $Z'$  or any form of the four-fermion contact interactions. This identification reach is numerically similar to the 95% CL *discovery* reach for graviton exchange obtained using only singly longitudinally polarized beams [92,94,95] for the same process. It is important that a more detailed study of this type be performed using a realistic detector simulation since the likely size of the true systematic errors will be somewhat larger than those assumed in this analysis. However, the reach here is so large it is clear that this is an avenue worth pursuing.

$E_{CM}$ (GeV)	Reach (TeV)
500	5.4
800	8.8
1000	11.1
1200	13.3
1500	16.7

Table 2.5: Identification reach for  $M_H$  in the ADD model assuming the distribution  $N^{-1}dA/dz \sim 1 - z^2$  and varying the individual normalizations for the final states  $f = \mu, \tau, f = b$  and  $f = c$  for LC of different center of mass energies.

Given these results we can go a step further. If graviton and  $Z'$  exchanges can be distinguished up to  $M_H \leq (10 - 11)\sqrt{s}$  using TP, what is the corresponding 95% CL search reach for graviton exchange obtainable with TP? For this type of analysis we assume that the  $N^{-1}dA/dz$  distributions for each final state fermion are given by their SM values and ask at what value of  $M_H$  the corresponding ones with graviton exchange become indistinguishable from these. Again we find that above very modest integrated luminosities the errors are completely dominated by systematics; we thus expect our results to again be on the high side of what would be obtained in a more detailed detector study. These results are shown in Table 2 where we see that the values are in the range  $M_H \geq 20\sqrt{s}$ . These are such enormous numbers that even a degradation by 30 – 40% would lead to the highest search reaches for KK graviton exchange found so far [95].

$E_{CM}$ (GeV)	Reach (TeV)
500	10.2
800	17.0
1000	21.5
1200	26.0
1500	32.7

Table 2.6: 95% CL search reach for  $M_H$  as described in the text.

Given the great sensitivity of transverse polarization to KK graviton/spin-2 exchange it would be natural to ask if TP can be used to distinguish the ADD from the RS model scenarios below KK production threshold. At first, there would seem to be no difference between the predictions of these two models for the situation under discussion. In the RS model, if we are away from the  $Z$  and graviton KK poles the imaginary part of amplitude which enters the term proportional to  $\sin 2\phi$  becomes vanishingly small. However, as was recently pointed out by Datta, Gabrielli and Mele [96], the exchange of an essentially continuous spectrum of ADD gravitons leads to a finite, cutoff-independent *imaginary* part of the amplitude. This forgotten piece grows very rapidly with increasing  $\sqrt{s}$  and depends quite sensitively upon the number of extra dimensions. Since this term is finite it directly probes the effective fundamental Planck scale of the extra-dimensional theory. Using the notation employed above one now finds that  $f_g$  has a grown imaginary part:

$$f_g = \frac{\lambda s^2}{4\pi\alpha M_H^4} \left[ 1 - i \frac{\pi M_H^4 (\sqrt{s})^{\delta-2} S_{\delta-1}}{16M_D^{\delta+2}} \right], \quad (35)$$

where  $\delta$  is the number of extra dimensions,  $M_D$  is the  $\delta$  dimensional fundamental scale and  $S_{\delta-1}$  is the area of the  $\delta$  sphere. We again note that the magnitude of this new imaginary part, unlike the real part as parameterized in the Hewett scheme, depends quite strongly on the number of extra dimensions.

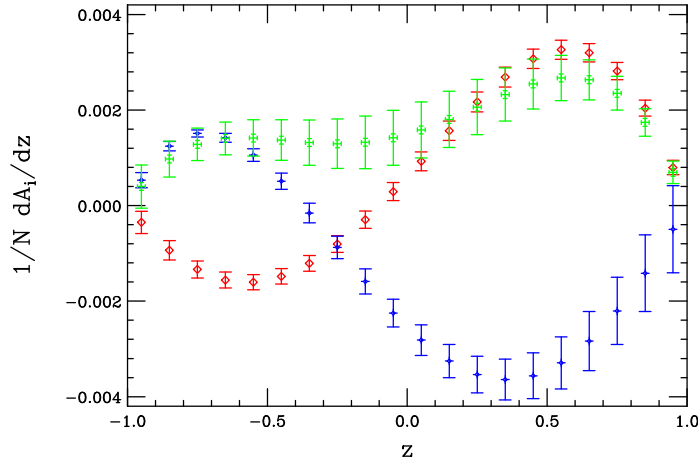


Figure 19: The  $N^{-1}dA_i/dz$  distributions at a 500 GeV collider assuming  $M_H = M_D = 1.5$  TeV and  $\delta = 3$  with an integrated luminosity of  $500 fb^{-1}$ . The plotted points from top to bottom in the center of the plot correspond to  $f = b, \mu$  plus  $\tau$  and  $c$ , respectively.

To proceed [97] we can form a new asymmetry in analogy to the above:

$$\frac{1}{N} \frac{dA_i}{dz} = \left[ \frac{\int_+ \frac{d\sigma}{dzd\phi} - \int_- \frac{d\sigma}{dzd\phi}}{\int d\sigma} \right], \quad (36)$$

where now the  $\int_{\pm}$  are integrations over regions where  $\sin 2\phi$  takes on  $\pm$  values and we integrate over all  $z$  and  $\phi$  in the denominator as before. We note that when we perform the integrations in this manner all terms proportional to  $\cos 2\phi$  are found to cancel implying that there is no cross contamination from this other asymmetry source. (This also implies

that all of our analyses above will go through even if a term proportional to  $\sin 2\phi$  is present.) Of course this new distribution is identically zero in both the SM as well as the RS model away from the  $Z$  and RS KK graviton poles. Thus, observing *any* non-zero value for this quantity is a signal for the ADD model. This is particularly true after the spin-2 nature of the exchange has already been established. Fig 4 shows how these new asymmetry distributions may appear at a 500 GeV LC assuming as before that  $P_T = 0.8$  and  $P'_T = 0.6$  and taking  $\delta = 3$  for purposes of demonstration. For simplicity we have assumed  $M_H = M_D$  in this figure and will continue to do so in our discussion below; we expect these two mass scales to be reasonably comparable, though if for some reason  $M_H \ll M_D$  this would lead to a serious modification in the sensitivity to this observable.

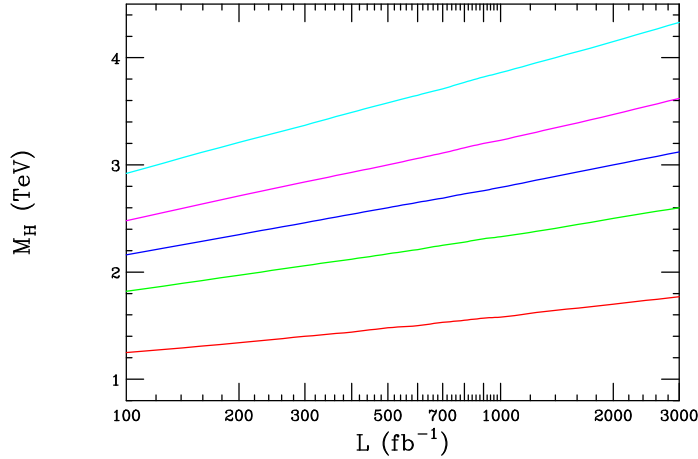


Figure 20:  $5\sigma$  reach for the discovery of a nonzero value of the azimuthal asymmetry  $N^{-1}dA_i/dz$  distribution as a function of the integrated luminosity at a LC for  $\delta = 3$ . From bottom to top the curves are for  $\sqrt{s} = 0.5, 0.8, 1, 1.2$  and  $1.5$  TeV, respectively.  $M_H = M_D$  is assumed throughout as is  $P_T = 0.8$  and  $P'_T = 0.6$ .

Assuming a value of  $\delta$  we can ask up to what value of  $M_H = M_D$  we can determine that the  $N^{-1}dA_i/dz$  distribution is non-zero at the  $5\sigma$  level. Based on the expression above we expect that this reach will be reasonably sensitive to the value of  $\delta$ ; this is indeed what we find from Fig. 5 which show the resulting reaches at the  $5\sigma$  level for the range  $\delta = 3$  which is  $\sim (2.5 - 3)\sqrt{s}$ . Although this number is not large in comparison to those we've obtained in the other analyses above they provide the first indication that these two scenarios can be distinguished at a collider via indirect measurements.

## Other Processes

Can useful limits be obtained from other processes? Figs. 6 and 7 show the effect of graviton exchange on the azimuthal asymmetry for the processes  $e^+e^- \rightarrow W^+W^-, \gamma\gamma$  and  $ZZ$ , respectively. In the  $W^+W^-$  case, the asymmetry is not symmetric in  $z$  in the SM so we can't use our shape fitting trick here as we did for fermions. Changes in the asymmetry shape in this case can come from all kinds of new physics and not just gravity. However, we find that the new physics reach from this process is  $M_H \sim 6 - 7\sqrt{s}$ . Note that for the other two processes new spin-1 exchanges are not possible so deviations must arise from higher dimensional operators. The search reaches in these cases is found to be in the  $M_H \sim 5 - 6\sqrt{s}$  range.

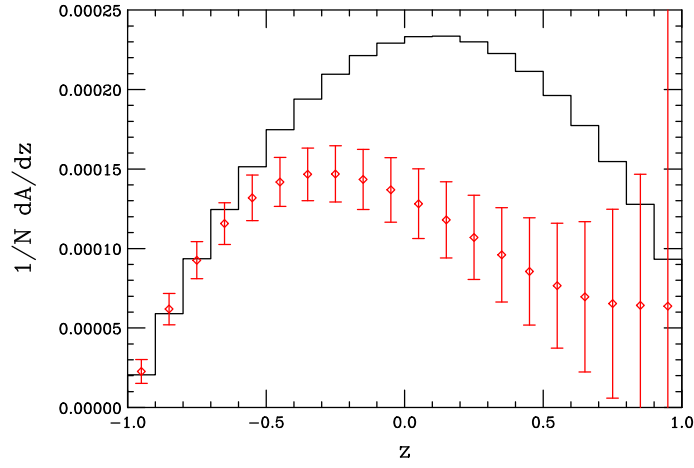


Figure 21: Transverse polarization asymmetry in  $e^+e^- \rightarrow W^+W^-$  at a 500 GeV LC with a luminosity of  $0.5 \text{ ab}^{-1}$ . The SM is the histogram while the data is for  $M_H = 2 \text{ TeV}$ .

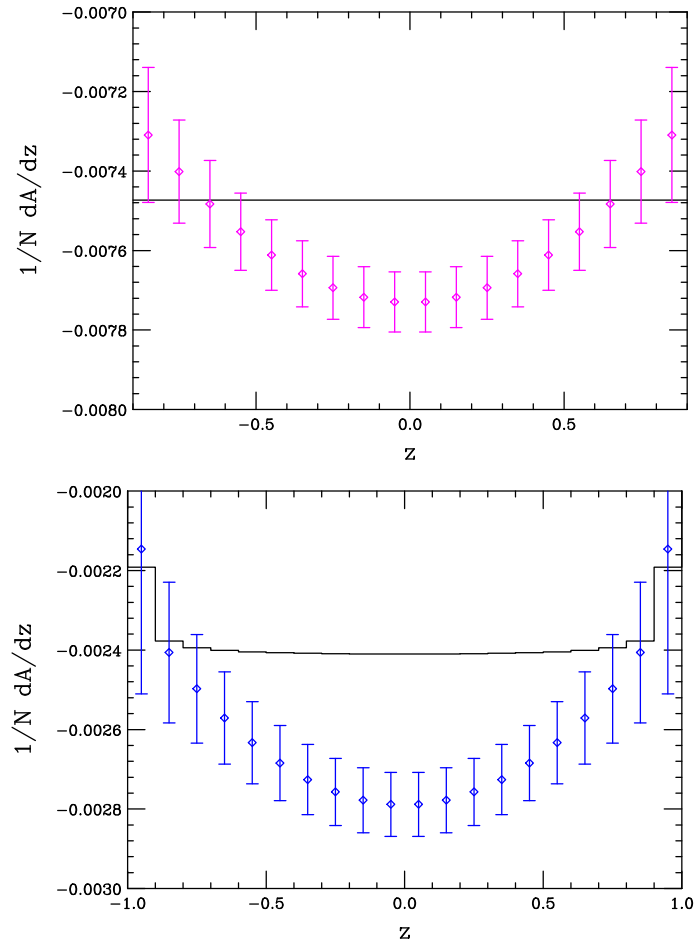


Figure 22: Same as the previous figure but now for  $e^+e^- \rightarrow \gamma\gamma(ZZ)$  in the top(bottom) panel.

## Summary and Conclusion

Historically, transverse polarization has not received much attention in the literature as a probe for new physics signatures. However, in searching for and identifying new physics at colliders one must make use of as many tools as possible.

In this paper we have examined the possible uses of transverse polarization in searching for, discovering and identifying spin-2 graviton exchange signatures in models with extra dimensions. The results of our analysis are as follows: (i) We have found that the interference of SM and spin-2 graviton KK exchanges leads to contributions to the azimuthal asymmetry distributions which are odd in  $\cos\theta$ , a rather unique signature. The appearance of such odd terms does not happen in the case of other new physics such as a  $Z'$ , contact interactions, gauge boson KK excitations or the exchange of new scalars. (ii) Using two different sets of observables that probe the integrated contributions of these odd terms, we showed that it possible to differentiate KK graviton/spin-2 exchanges from all other new physics contributions to contact interactions at the  $5\sigma$  level up to ADD cutoff scales of  $M_H \sim (3.5 - 4)\sqrt{s}$ . (iii) Fitting to the shape of the full differential distribution itself was shown to provide much more discriminating power; we found that the  $5\sigma$  identification reach was substantially increased to  $M_H = (10 - 11)\sqrt{s}$ , about a factor two improvement over what we obtained in our earlier analysis in the case of longitudinal polarization. This result is, however, quite sensitive to our assumptions about the sizes of various systematic errors. (iv) Using this same type of analysis we obtained a 95% CL search reach for new physics in excess of  $m_H = 20\sqrt{s}$ ; this is again about a factor of two improvement over other analyses. As in the previous analysis, this result is also quite sensitive to the assumed values of the systematic errors. Clearly, more detailed studies are required to verify these results. (v) In the case of the ADD model, an additional imaginary piece of the amplitude is present in comparison to the RS model below KK production threshold. We showed that this leads to a new asymmetry, produced through transverse polarization, which allows RS and ADD model separation at  $5\sigma$  up to masses  $M_H = (2.5 - 3)\sqrt{s}$ .

It is clear from our analysis that transverse polarization can be a very powerful tool in identifying new physics, particularly in the case of extra dimensions. Further detailed study of the effects examined here may prove extremely useful for future linear collider experiments.

## 2.14 Separation of light flavors with transverse polarisation

When both the electron and the positron beams are transversely polarized, a separation in space of quarks of different flavours  $f$  ( $u$ -type vs.  $d$ -type) is possible [98]. This effect comes about since the annihilation cross section has an azimuthal dependence (w.r.t. the beam polarization) which is flavour dependent.

Ignoring here the forward-backward asymmetry (since we shall integrate over a forward-backward symmetric interval in  $\cos \theta$ ), the electroweak annihilation cross section takes the form

$$\frac{d^2\sigma_f}{d\cos\theta d\phi} = \frac{3}{4} \frac{\alpha^2}{s} \left[ h_f^{(1)}(s)(1 + \cos^2\theta) + h_f^{(3)}(s)P_+^\perp P_-^\perp \sin^2\theta \cos(2\phi - \phi_+ - \phi_-) \right], \quad (37)$$

with  $\theta$  and  $\phi$  polar and azimuthal angles of the quark momentum. The energy- and flavour-dependent functions  $h_f^{(1)}(s)$  and  $h_f^{(3)}(s)$  are given by

$$\begin{aligned} h_f^{(1)}(s) &= Q_f^2 - 2Q_f v v_f \text{Re}\chi(s) + (v^2 + a^2)(v_f^2 + a_f^2)|\chi(s)|^2, \\ h_f^{(3)}(s) &= Q_f^2 - 2Q_f v v_f \text{Re}\chi(s) + (v^2 - a^2)(v_f^2 + a_f^2)|\chi(s)|^2, \end{aligned} \quad (38)$$

with

$$\chi(s) = \frac{1}{4\sin^2 2\theta_W} \frac{s}{s - M_Z^2 + iM_Z\Gamma_Z}, \quad (39)$$

and  $M_Z$  and  $\Gamma_Z$  the mass and width of the  $Z$ . Furthermore,  $Q_f$  is the quark charge, and the electroweak coupling constants are normalized as

$$\begin{aligned} e^- : \quad v &= -1 + 4\sin^2 2\theta_W, & a &= 1, \\ u : \quad v_u &= 1 - \frac{8}{3}\sin^2 2\theta_W, & a_u &= 1, & Q_u &= \frac{2}{3} \\ d : \quad v_d &= -1 + \frac{4}{3}\sin^2 2\theta_W, & a_d &= -1, & Q_d &= -\frac{1}{3}. \end{aligned} \quad (40)$$

The effect of flavour separation is thus related to the fact that the ratio  $h_f^{(3)}(s)/h_f^{(1)}(s)$  depends on the flavour  $f$ . The effect is maximum for polar angle  $\theta = \pi/2$ . If one integrates over some range in polar angle, centered around  $\theta = \pi/2$ , one finds

$$\begin{aligned} \frac{d\sigma_f(\theta_0, \phi)}{d\phi} &= \int_{-\cos\theta_0}^{\cos\theta_0} \frac{d^2\sigma_f}{d\cos\theta d\phi} d\cos\theta \\ &= \frac{3\alpha^2}{2s} \cos\theta_0 \left( 1 + \frac{1}{3}\cos^2\theta_0 \right) \left[ h_f^{(1)}(s) + h_f^{(3)}(s)\xi \cos(2\phi - \phi_+ - \phi_-) \right], \end{aligned} \quad (41)$$

with

$$\xi = P_+^\perp P_-^\perp \frac{1 - \frac{1}{3}\cos^2\theta_0}{1 + \frac{1}{3}\cos^2\theta_0}. \quad (42)$$

Flavour separation is then achieved in the sense that the ratio

$$R_{u/d}(\phi) = \frac{d\sigma_u(\theta_0, \phi)}{d\sigma_d(\theta_0, \phi)} = \frac{h_u^{(1)}(s) + h_u^{(3)}(s)\xi \cos(2\phi - \phi_+ - \phi_-)}{h_d^{(1)}(s) + h_d^{(3)}(s)\xi \cos(2\phi - \phi_+ - \phi_-)} \quad (43)$$

becomes  $\phi$ -dependent. This ratio is shown in Fig. 23, for  $\cos\theta_0 = 0.5$  (integrated over  $\pi/3 \leq \theta \leq 2\pi/3$ ) and for degrees of transverse polarization 1.0 and 0.8. Mass effects tend to make the distribution more isotropic, and thus reduce the degree of separation [98].

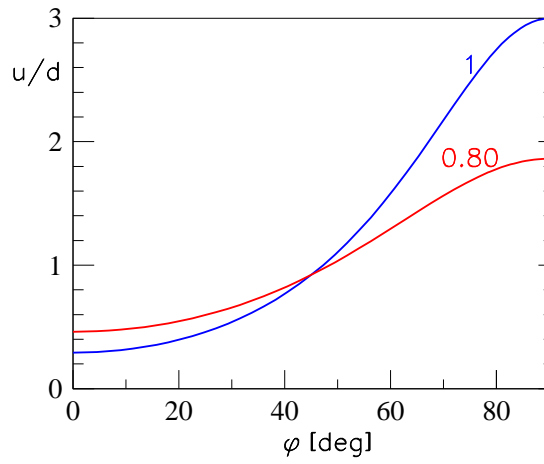


Figure 23: Flavour separation at  $\sqrt{s} = 0.5$  TeV:  $u/d$  vs azimuthal angle, for the range  $\pi/3 \leq \theta \leq 2\pi/3$ , and for transverse degrees of polarization 1 and 0.80, as indicated.

## 2.15 Polarisation Measurement: GigaZ – Precision tests of the electroweak theory

### 2.15.1 Introduction

The option GigaZ refers to running the LC at the Z resonance with to about  $10^9$  Z events and makes possible the most sensitive test of the SM ever made.

In the SM the left–right asymmetry  $A_{LR}$  depends only on the effective leptonic weak mixing angle:

$$A_{LR} = \frac{2(1 - 4 \sin^2 \Theta_{eff}^l)}{1 + (1 - 4 \sin^2 \Theta_{eff}^l)^2}. \quad (44)$$

The statistical power of the data sample can be fully exploited only when  $\delta(A_{LR}(pol)) < \delta(A_{LR}(stat))$ . For  $10^8 - 10^9$  Z's this occurs when  $\delta(P_{eff}) < 0.1\%$ . In this limit  $\delta(\sin^2 \theta_{eff}) \sim 10^{-5}$ , which is an order-of-magnitude smaller than the present value of this error. Thus it will be crucial to minimize the error in the determination of the polarization. Although the improvements in Compton polarimetry achieving a precision  $< 0.1\%$  may be difficult. The desired precision should, nevertheless, be attainable with the Blondel Scheme, where it is not necessary to know the beam polarization with such extreme accuracy, since  $A_{LR}$  can be directly expressed via cross sections for producing Z's with longitudinally polarized beams:

$$\sigma = \sigma_{unpol}[1 - P_{e^-}P_{e^+} + A_{LR}(P_{e^+} - P_{e^-})], \quad (45)$$

$$A_{LR} = \sqrt{\frac{(\sigma^{RR} + \sigma^{RL} - \sigma^{LR} - \sigma^{LL})(-\sigma^{RR} + \sigma^{RL} - \sigma^{LR} + \sigma^{LL})}{(\sigma^{RR} + \sigma^{RL} + \sigma^{LR} + \sigma^{LL})(-\sigma^{RR} + \sigma^{RL} + \sigma^{LR} - \sigma^{LL})}}. \quad (46)$$

In this formula the absolute polarisation values of the left- and the right-handed states are assumed to be the same. Corrections have to be determined experimentally by means of polarimetry techniques; however, only relative measurements are needed, so that the absolute calibration of the polarimeter cancels [3].

As can be seen from (46) the Blondel scheme also requires some luminosity for the less favoured combinations (LL, RR). However only about 10% of running time will be needed for these combinations to reach the desired accuracy for these high precision measurements. Fig. 24 shows the statistical error on  $A_{LR}$  as a function of the positron polarisation for  $P_{e^-} = 80\%$ . Already with 20% positron polarisation the goal of  $\delta \sin^2 \theta_{eff} \sim 10^{-5}$  can be reached. The comparison of different beam polarisation configurations and the gain for the  $A_{LR}$  Measurements see also [4].

As an example of the potential of the GigaZ  $\sin^2 \theta_{eff}$  measurement Fig. 25 compares the present experimental accuracy on  $\sin^2 \theta_{eff}$  and  $M_W$  from LEP/SLD/Tevatron and the prospective accuracy from the LHC and from a LC without GigaZ option with the predictions of the SM and the MSSM. With GigaZ a very sensitive test of the theory will be possible.

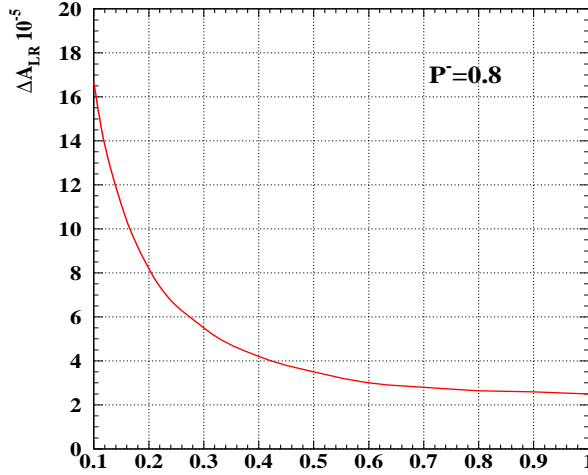


Figure 24: Test of Electroweak Theory: The statistical error on the left–right asymmetry  $A_{LR}$  of  $e^+e^- \rightarrow Z \rightarrow \ell\bar{\ell}$  at GigaZ as a function of the positron polarization  $P(e^+)$  for fixed electron polarization  $P_{e^-} = \pm 80\%$  [3].

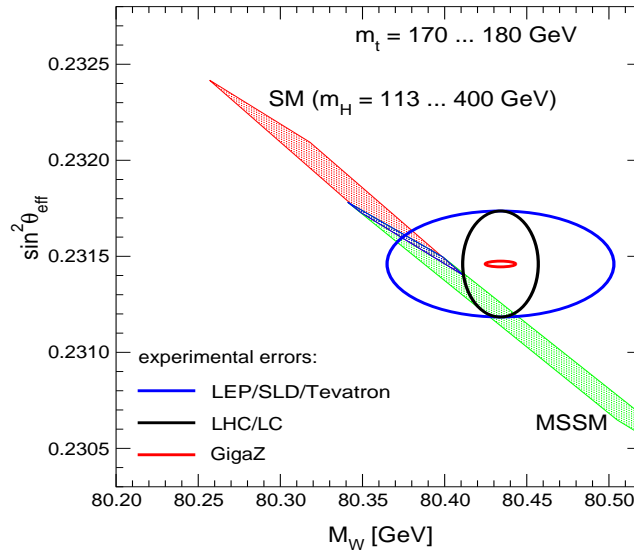


Figure 25: Test of Electroweak Theory: A high-precision measurement at GigaZ of the left–right asymmetry  $A_{LR}$  and consequently of  $\sin^2 \Theta_{eff}^l$  allows to test the electroweak theory at an unprecedented level. The allowed parameter space of the SM and the MSSM in the  $\sin^2 \Theta_{eff}^l - M_W$  plane is shown together with the experimental accuracy reachable at GigaZ. For comparison, the present experimental accuracy (LEP/SLD/Tevatron) and the prospective accuracy at the LHC and a LC without GigaZ option (LHC/LC) are also shown [5,6].

## 2.15.2 Higgs mass versus electroweak mixing angle

The precise measurement of the effective leptonic weak mixing angle at the Z-boson resonance,  $\sin^2 \theta_{\text{eff}}$ , at GigaZ will allow a very sensitive test of the electroweak theory [6]. With both beams polarized, i.e. 80% polarization for electrons and 60% polarization for positrons, an accuracy of  $\Delta \sin^2 \theta_{\text{eff}} = \pm 1.3 \times 10^{-5}$  can be achieved [7]. If only electron polarization were available, this would result in an accuracy of only about  $\Delta \sin^2 \theta_{\text{eff}} = \pm 9.5 \times 10^{-5}$  [8].

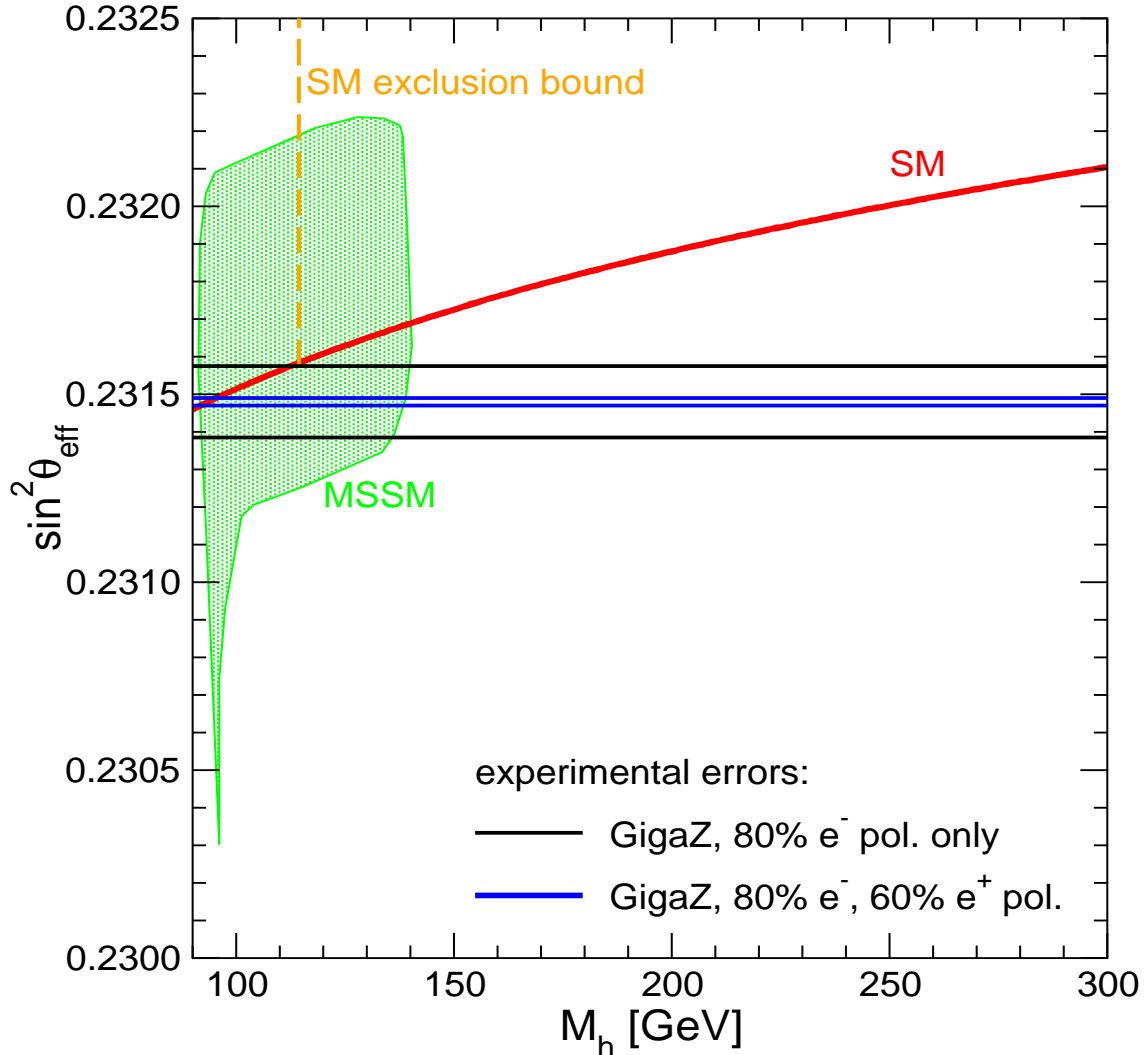


Figure 26: The predictions for  $\sin^2 \theta_{\text{eff}}$  in the SM and the MSSM as a function of  $M_h$ , which corresponds to the Higgs-boson mass in the SM and the mass of the lightest  $\mathcal{CP}$ -even Higgs boson in the MSSM. The exclusion bound on the SM Higgs mass of  $M_h > 114.4$  GeV [9] is indicated in the plot. The SM prediction is given for  $m_t = 175 \pm 0.1$  GeV, while in the MSSM the SUSY parameters have been scanned. The theory predictions are compared with the experimental accuracies obtainable at GigaZ with an 80% polarized electron beam only and with the case of simultaneous polarization of both beams.

The impact of the more precise measurement for testing the electroweak theory is indicated in Fig. 26, where the experimental accuracy (using the current experimental central

value of  $\sin^2 \theta_{\text{eff}}$  [10]) is compared with the predictions in the SM and the MSSM. The theoretical predictions are shown as a function of  $M_h$ , which corresponds to the Higgs-boson mass in the SM and the mass of the lightest  $\mathcal{CP}$ -even Higgs boson in the MSSM. In the region where both models overlap,  $M_h \lesssim 135$  GeV [11], the SM prediction corresponds to the MSSM result in the limit where all SUSY partners are heavy. The area corresponding to the MSSM prediction was obtained by varying all relevant SUSY parameters independently, taking into account the constraints from the direct search for SUSY particles and the LEP Higgs search. The MSSM predictions are based on the results described in Ref. [12], and the Higgs mass predictions have been obtained with *FeynHiggs2.0* [13]. Within the SM, the precision in  $\sin^2 \theta_{\text{eff}}$  achievable with both beams polarized constrains the Higgs-boson mass to an interval of few GeV (neglecting the uncertainties from unknown higher-order corrections), while the precision corresponding to electron polarization leaves an uncertainty of about  $\pm 25$  GeV in  $M_h$ . Within the MSSM the parameter space in the  $M_h$ - $\sin^2 \theta_{\text{eff}}$  plane is reduced by about a factor 7 with the  $\sin^2 \theta_{\text{eff}}$  measurement based on simultaneous polarization of both beams as compared to the case with electron polarization only. This puts sensitive constraints on the possible values of the underlying SUSY parameters. Combined with direct information on the SUSY spectrum the precise measurement of  $\sin^2 \theta_{\text{eff}}$  will allow a very stringent consistency test of the MSSM.

## 2.16 Summary of the Physics Cases

We agreed in the POWER meeting that we should provide a table (like table 1 in GMP, Steiner, hep-ph/0106155) summarising (also quantitatively) the effects of having  $P(e^+)$  in addition to  $P(e^-)$ .

## Chapter 3

# Implementation of Spin Effects in Monte Carlo Generators

The use of numerical programs based on Monte Carlo (MC) techniques has become essential in performing any detailed experimental analysis in collider physics. In this section we will briefly recall the key features of these programs and discuss the inclusion of beam polarization effects. We will limit ourselves to the so-called event generators. These programs must be interfaced to both detector simulations and beam energy spectra to give a complete picture of the actual physics process.

In general the MC event generation process can be split into a number of phases.

- The hard process where the particles in the hard collision and their momenta are generated, usually according to the leading-order scattering matrix element (ME).
- The parton-shower (PS) phase where the coloured particles in the event are perturbatively evolved from the hard scale of the collision to the infrared cut-off. The emission of electromagnetic radiation from charged particles can be handled in a similar way.
- Those particles which decay before hadronization, *e.g.* the top quark, are decayed usually according to a calculated branching ratio with a ME to give the momenta of the decay products. Any coloured particles produced in these decays are then evolved by the PS algorithm.
- A hadronization phase in which the partons left after the perturbative evolution are formed into the observed hadrons.

Most MC event generators fall into one of two classes: *general-purpose (or multi-purpose) event generators* which aim to perform the full simulation of the event starting with the initial-state collider beams, proceeding through the hard scattering process and finishing with the final-state hadrons; the second class of programs (hereafter, *parton-level event generators*) typically performs the hard scattering part of the simulation only, perhaps including decays, and relies on one of the general-purpose generators for the rest of the simulation.

During the LEP-era the experiments relied on the general-purpose event generators for the description of hadronic final states together with more accurate parton-level programs

interfaced to the former ones for specific processes, *e.g.* two- and four-fermion production. At a future linear collider (LC), as one wishes to study final states with higher multiplicities, for example six or even eight particles, this mixed approach will become more important as these final states cannot be described by the general-purpose event generators.

### 3.1 General-purpose Event Generators

Historically the main general-purpose event generators have been HERWIG [99], ISAJET [100] and PYTHIA [101]. While the general philosophy of these programs is similar, they use different phenomenological models and approximations. In general, at least for  $e^+e^-$  collisions, the range of hard scattering processes implemented is very similar. All these generators have a wide range of Standard Model (SM) processes available, reactions predicted by the Minimal Supersymmetric Standard Model (MSSM) as well as various selections of channels from other models too (*e.g.* extra gauge-bosons).

The major differences between the programs are in the approximations used in the PS evolution and the hadronization stage. While ISAJET still adopts the original PS algorithm which only re-sums collinear logarithms, both HERWIG and PYTHIA include the effects of soft logarithms via either an angular-ordered PS in the case of HERWIG, or an angular veto in the case of PYTHIA. For the hadronization process HERWIG uses the cluster model, ISAJET the independent fragmentation model and PYTHIA the Lund string model.

There are also major differences between the generators in the treatment of spin correlation and polarization effects. Both ISAJET and HERWIG include longitudinal polarization effects in both SM and Supersymmetric (SUSY) production processes, while PYTHIA includes both longitudinal and transverse polarizations in many processes. Another important difference is in the treatment of the subsequent decay of any heavy particle produced in the hard process. While HERWIG includes the full correlations in any subsequent decays using the method described in [102] both ISAJET and PYTHIA only include these effects in some processes, *e.g.*  $W$  pair production. To extend the method used in [102] to include transverse polarization also in the HERWIG production stage is certainly possible.

While these codes will continue to be used in the near future a major programme is underway to produce a new generation of general-purpose event generators in C++. The main aim of it is to provide the tools needed for the Large Hadron Collider (LHC). However, these tools will be used also for the next generation of LCs. The only program currently available in C++ which is capable of generating physics results is SHERPA (based on the APACIC++ [103] PS). Work is however underway to rewrite both PYTHIA [104] and HERWIG [105] in C++. These programs should be available in the next few years and we expect them to be the major tools for event generator at a future LC. Given the new design and structure of these programs the treatment of both spin correlation and polarization effects should be much better than in the current FORTRAN programs. For example HERWIG++, should include full polarization and correlation effects in the perturbative phase of the event using the method of [102].

## 3.2 Parton-Level Event Generators

There are a large number of programs available which calculate an individual hard process, or some set of hard processes, and are interfaced to one of the general-purpose generators, most often PYTHIA, to perform the PS and hadronization. It is impossible to review all such programs here. As many of the two- [106] and four-fermion [107] generators were used by the LEP collaborations, we refer to the report of the LEP-II MC workshop for their detailed discussion. Some programs, *e.g.*, LUSIFER [108], SIXFAP [109], EETT6F [110] and SIXPHACT [111], have been written specifically for six fermion processes. Many of these codes use helicity amplitude techniques to calculate the MEs and therefore either already include polarization effects or could easily be modified to do so. Given the vast physics programme of future LCs, it is likely that one will also regularly resort to programs which are capable of calculating and integrating the MEs for large numbers of final-state particles automatically. There are a number of such codes available.

- AMEGIC++ [112] makes use of helicity amplitude techniques to evaluate the ME together with efficient multi-channel phase space integration to calculate the cross section. This package is part of SHERPA.
- COMPHEP [113] is an automatic program for calculation of cross sections for processes with up to eight external particles\*. It uses the traditional trace techniques to evaluate the ME together with a modified adaptive integrator to compute the cross section, so it is at present not suitable for studies intended to investigate polarization/spin effects. However, the conversion to the use of helicity amplitudes techniques is currently planned.
- GRACE [114] (with the accompanying packages BASES and SPRING) combines the calculation of MEs via helicity amplitude techniques with adaptive integration.
- HELAC/PHEGAS uses the approach of [115] which is based on the Dyson-Schwinger equation together with multi-channel integration [116] to calculate the cross section.
- MADGRAPH/MADEVENT [117] uses helicity amplitude techniques for the ME together with an efficient multi-channel phase space integrator to compute the cross section. These packages are based on the HELAS [118] subroutines.
- WHIZARD [119] is a multi-channel integration package which can use either COMPHEP, MADGRAPH or O' MEGA† [121] to calculate the MEs.

All of these codes apart from HELAC/PHEGAS‡ are publicly available. In order to simulate events these programs need to be interfaced to the general-purpose event generators. Most use *ad hoc* interfaces to one of the major general-purpose event generators with the details varying from one package to another. Recently, generic (*i.e.*, program-independent) FORTRAN common blocks have been proposed for the transfer of event configurations from parton level programs to showering and hadronization event generators [122].

The implementation of polarization and correlation effects differs between these programs. In general, apart from COMPHEP (as noted), these programs are all based on helicity amplitude techniques at some point in the calculation and therefore the inclusion of both transverse and longitudinal beam polarization is possible even where it is not currently implemented.

---

\*COMPHEP can have up to six final-state particles for scattering processes and seven for decays.

†O' MEGA uses the approach of [120] to evaluate the ME but does not include yet any QCD processes.

‡Contact: papadopo@alice.nuclear.demokritos.gr.

### 3.3 SUSY

Polarization and spin correlation effects are particularly important in studying SUSY scenarios, in order to measure the fundamental parameters of the underlying model. Thus, it is worth commenting in more detail on the inclusion of these effects in SUSY processes (hereafter, we assume the particle content of the MSSM).

HERWIG, PYTHIA and ISAJET all include longitudinal polarization effects in SUSY production processes. There is also a parton-level program SUSYGEN [123], interfaced to PYTHIA, which includes these effects.

All these programs also differ in the inclusion of the correlations in the subsequent decays of the particles. While SUSYGEN includes these correlations using helicity amplitude techniques and HERWIG uses the method of [102], these effects are generally not included in either PYTHIA or ISAJET.

Among the parton-level programs, at present only COMPHEP and GRACE include SUSY processes, although both MADGRAPH and AMEGIC++ can be extended to add the additional interactions which are needed.

# Chapter 4

## Machine Issues

### 4.1 Electron Polarisation

Author: Jim Clendenin

### 4.2 Positron Polarisation

Contributions from John Sheppard and Tsunehiko Omori

Contribution from Daresbury lab (D. Scott, J. Clarke) already arrived, but not yet in latex style transformed (see next page)

# Chapter 5

## Polarisation Measurement

Contribution from Peter Schueler

Contribution from Mike Woods and Ken Moffeit already arrived, but not yet in latex style transformed (see next pages)